JOURNAL OF PETROLOGY | VOLUME 41 | NUMBER 1 | PAGES 21–42 | 2000

# Remobilization of Andesite Magma by Intrusion of Mafic Magma at the Soufriere Hills Volcano, Montserrat, West Indies

**M. D. MURPHY[1]*, R. S. J. SPARKS[1], J. BARCLAY[1,2], M. R. CARROLL[1,3] AND T. S. BREWER[4]**

[1] DEPARTMENT OF EARTH SCIENCES, UNIVERSITY OF BRISTOL, WILLS MEMORIAL BUILDING, QUEENS ROAD, BRISTOL BS8 1RJ, UK

[2] DÉPARTEMENT DE MINÉRALOGIE, UNIVERSITÉ DE GENÈVE, 13 RUE DES MARAICHERS, 1211 GENEVA 4, SWITZERLAND

[3] DIPARTIMENTO DI SCIENZE DELLA TERRA, UNIVERSITÁ DI CAMERINO, 62032 CAMERINO, ITALY

[4] GEOLOGY DEPARTMENT, UNIVERSITY OF LEICESTER, UNIVERSITY ROAD, LEICESTER LE1 7RH, UK

**RECEIVED SEPTEMBER 3, 1998; REVISED TYPESCRIPT ACCEPTED JUNE 14, 1999**

*The 1995–1999 eruption of the Soufriere Hills volcano, Montserrat, has produced a crystal-rich andesite containing quench-textured mafic inclusions, which show evidence of having been molten when incorporated into the host magma. Individual crystals in the andesite record diverse histories. Amphibole phenocrysts vary from pristine and unaltered to strongly oxidized and pseudomorphed by anhydrous reaction products. Plagioclase phenocrysts are commonly reverse zoned, often with dusty sieve textures. Reverse zoned rims are also common on orthopyroxene phenocrysts. Pyroxene geothermometry gives an average temperature of 858 ± 20°C for orthopyroxene phenocryst cores, whereas reverse zoned rims record temperatures from about 880 to 1050°C. The heterogeneity in mineral rim compositions, zoning patterns and textures is interpreted as reflecting non-uniform reheating and remobilization of the resident magma body by intrusion of hotter mafic magma. Convective remobilization results in mixing together of phenocrysts that have experienced different thermal histories, depending on proximity to the intruding mafic magma. The low temperature and high crystallinity are interpreted as reflecting the presence of a cool, highly crystalline magma body beneath the Soufriere Hills volcano. The petrological observations, in combination with data on seismicity, extrusion rate and $SO_2$ fluxes, indicate that the current eruption was triggered by recent influx of hot mafic magma.*

KEY WORDS: *Montserrat; eruption; magma mixing; mafic inclusion; sieve texture*

## INTRODUCTION

The Soufriere Hills volcano, Montserrat, located in the Lesser Antilles island arc in the West Indies, began to erupt on 18 July 1995, after about 350 years of dormancy (Young *et al.*, 1998*b*). The eruption was preceded by a period of seismic swarms, which began in January 1992. Previous earthquake crises have occurred on Montserrat in 1896–1897, 1932–1935 and 1966–1967 (Powell, 1938; Shepherd *et al.*, 1971). Initial phreatic and phreatomagmatic activity was followed by extrusion of an andesitic lava dome in November 1995. Pyroclastic flows, generated by gravitational collapse of the unstable dome, have been the dominant form of activity throughout the eruption, but periods of explosive activity, producing pumice flows and falls, have also occurred (Robertson *et al.*, 1998; Young *et al.*, 1998*b*). Dome growth ceased suddenly in March 1998 and further activity up to May 1999 has mainly involved gravitational collapses of the dome and periods of ash venting, with some small-scale vulcanian explosive events.

The Soufriere Hills volcano is the only active centre on Montserrat. The volcano is a composite of at least five andesitic lava domes, flanked by pyroclastic deposits. Rea (1974) identified four other volcanic centres, all inactive, the oldest dating back to about 4·5 Ma. Andesite

*Corresponding author. Present address: English Nature, Northminster House, Peterborough PE1 1UA, UK.

is the predominant eruptive product of all of the inactive centres, except for the South Soufriere Hills centre, which produced mainly basalt and basaltic andesite (Rea, 1974; Baker, 1984). The South Soufriere Hills centre was active at about 125 ka, coeval with early activity at the nearby Soufriere Hills volcano (Harford *et al.*, in preparation).

The petrology and geochemistry have been monitored throughout the current eruption (Devine *et al.*, 1998*a*, 1998*b*; Murphy *et al.*, 1998). The rock is a coarse-grained, porphyritic, crystal-rich, hornblende–hypersthene andesite, which has shown no consistent variation in bulk chemistry since the beginning of the eruption. Lithologic types include grey to reddened poorly vesicular lava, and moderately to highly vesicular pumice. There is no correlation between rock type and bulk chemical variation. Rare banded lava and pumice generally show no significant difference in composition between layers. Basaltic to basaltic andesite inclusions, which range in size from <1 mm to about 40 cm, form a minor (<1 wt %) but ubiquitous component of the andesite (Murphy *et al.*, 1998). These mafic inclusions show evidence for having been molten when incorporated into the andesite, and phenocrysts in the andesite show evidence for a recent reheating event.

In this paper, we describe the petrology and geochemistry of the andesite and mafic inclusions. We suggest that mineral heterogeneity within the andesite and the presence of mafic inclusions reflect remobilization of a relatively old, cool (~850°C), highly crystalline magma body by intrusion of hotter mafic magma. This process results in mechanical mixing of crystals that have experienced very different petrogenetic histories within the same magma body. We also suggest that the current eruption was triggered by recent intrusion of mafic magma into the system.

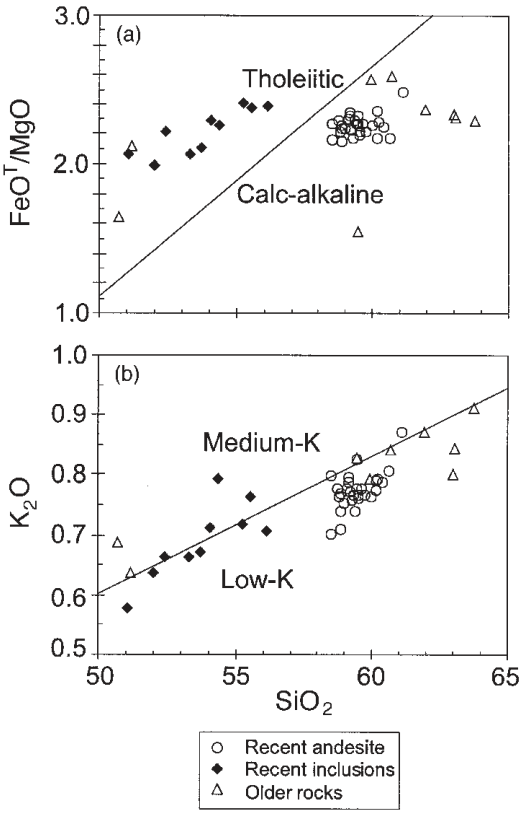


**Fig. 1.** Whole-rock classification diagrams after Miyashiro (1974) and Gill (1981). All samples plotted have been normalized to 100% volatile free with total Fe calculated as FeO.

## ANALYTICAL TECHNIQUES

X-ray fluorescence (XRF) analyses were performed at Leicester University using standard techniques described by Harvey *et al.* (1996). Analyses of international reference materials indicate that accuracy and precision are better than 0·5% for major elements and better than 3% for trace elements.

Electron microprobe analyses were performed at Bristol University on a JEOL JXA-8600 four-spectrometer instrument with LINK analytical X-ray analysis system and LEMAS automation. Online data reduction used the ZAF model. Run conditions were 15 kV accelerating voltage, beam current of 15 nA and minimum probe diameter (~1 μm). Counting times were 15 s on the peak and 8 s on the background. Accuracy and precision for most elements are better than 2–3% relative. In the case of Ca in orthopyroxene, important for pyroxene thermometry, repeat analyses are within 0·05 wt % CaO (absolute).

## GEOCHEMISTRY

Representative whole-rock major and trace element analyses of andesite and separated mafic inclusions, erupted between December 1995 and January 1998, are given in Table 1 and plotted in Figs 1 and 2. Analyses of older Soufriere Hills samples, ranging in age from about 350 years to 110 ka, and of a basaltic lava sample from the extinct South Soufriere Hills centre are also presented. All discussion here refers to analyses that have been normalized to 100% volatile free with total iron ($FeO^T$) calculated as FeO.

The current andesite averages 59·7 wt % $SiO_2$, with an overall between 58·4 and 62·4 wt % $SiO_2$ from 47 samples. Only three samples have $SiO_2$ contents higher than 61 wt %. There have been no systematic changes in bulk composition since the beginning of the eruption. Older Soufriere Hills rocks extend to slightly higher $SiO_2$ (63·8 wt %) than the current andesite. Mafic inclusions

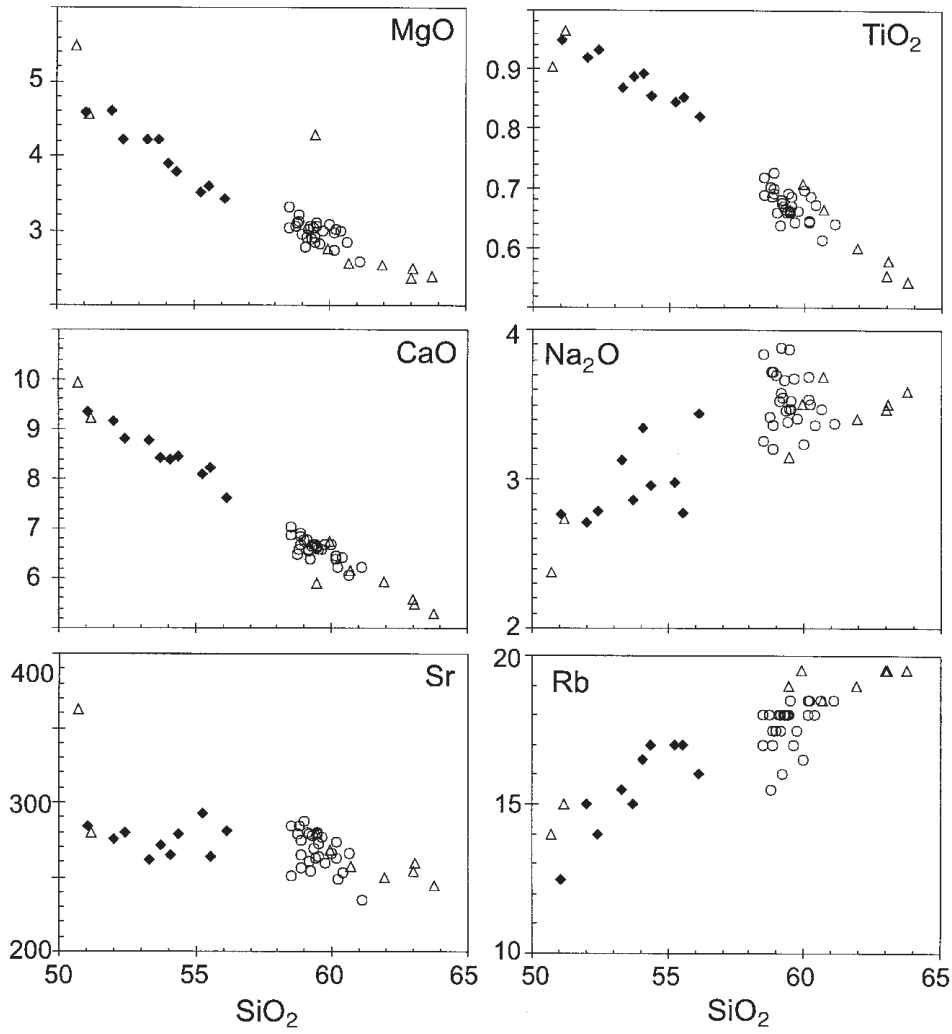


**Fig. 2.** Whole-rock variation diagrams with symbols as in Fig. 1.

from the current andesite typically have $SiO_2$ contents between 51 and 54 wt %, overlapping in composition with older South Soufriere Hills lava samples [Table 1; see Table 2 of Baker (1984)]. Some mafic inclusions extend to higher $SiO_2$ values (55–56% $SiO_2$) as a result of bulk incorporation of host andesite.

The Montserrat rocks are low K according to the classification of Gill (1981) (Fig. 1a). The mafic rocks plot in the tholeiite field of Miyashiro (1974), whereas the andesites plot in the calc-alkaline field (Fig. 1b). The mafic inclusions have MgO between 3·8 and 4·6 wt % and have very low Ni and Cr contents (Table 1). Compatible (MgO, $Al_2O_3$, CaO, $FeO^T$, $TiO_2$, Sr) and incompatible ($K_2O$, Rb, Ba, Zr) element abundances are higher and lower respectively in the andesites than in the mafic rocks, consistent with derivation of the andesite by fractionation from mafic magma of similar composition to the more mafic inclusions.

## ANDESITE PETROLOGY

The andesite is highly crystalline, consisting of about 45–55 wt % phenocrysts (>300 μm) and microphenocrysts (~100–300 μm), and 20–32 wt % microlites (<100 μm). The 100 μm limit on the size of microlites is arbitrary and defines the minimum size of crystals that can be point-counted accurately by optical microscopy. The upper limit on the size of microphenocrysts corresponds approximately to the maximum size of clinopyroxene crystals and also corresponds to a compositional change in plagioclase core compositions, as plagioclase crystals smaller than 250–300 μm are often significantly more calcic than the cores of larger phenocrysts.

The andesite contains about 30–35 wt % of plagioclase phenocrysts and microphenocrysts (Table 1). The other phenocrysts are amphibole (6–10 wt %), orthopyroxene

*Table 1: Representative whole-rock analyses*

| Sample no.: | MVO34 | MVO47 | MVO201 | MVO237 | MVO231 | MVO332 | MVO61 | MVO62 | MVO107 | MVO108 | MVO112 | MVO115 | MMON32 | MVO26 | MVO25 | MVO37 | MMON17 |
|---|---|---|---|---|---|---|---|---|---|---|---|---|---|---|---|---|---|
| Rock type: | Lava | Lava | Lava | Pumice | Lava | Lava | MI | MI | MI | MI | MI | MI | Lava | MI | Lava | Pumice | Pumice |
| Erupted: | Jan 96 | Aug 96 | Mar 97 | Jun 97 | Jul 97 | Dec 97 | May 96 | May 96 | Oct 96 | Oct 96 | Oct 96 | Oct 96 | ~125 ka | ~350 a | ~350 a | ~3·7 ka | ~18 ka |
| $SiO_2$ | 59·13 | 60·12 | 59·08 | 59·62 | 59·15 | 58·15 | 51·66 | 50·54 | 53·56 | 54·93 | 53·68 | 52·68 | 50·20 | 50·61 | 59·49 | 63·04 | 63·42 |
| $TiO_2$ | 0·63 | 0·65 | 0·62 | 0·60 | 0·63 | 0·63 | 0·86 | 0·84 | 0·71 | 0·72 | 0·80 | 0·76 | 0·88 | 0·88 | 0·59 | 0·55 | 0·55 |
| $Al_2O_3$ | 18·29 | 17·29 | 18·09 | 17·83 | 18·01 | 18·10 | 19·55 | 19·98 | 18·76 | 18·33 | 18·47 | 19·05 | 19·57 | 19·72 | 17·20 | 17·39 | 16·57 |
| $Fe_2O_3$ | 7·50 | 7·42 | 7·30 | 6·71 | 7·35 | 7·53 | 10·14 | 10·44 | 9·37 | 9·38 | 9·85 | 9·53 | 9·94 | 10·61 | 7·79 | 6·17 | 6·00 |
| MnO | 0·19 | 0·18 | 0·18 | 0·17 | 0·18 | 0·18 | 0·20 | 0·21 | 0·19 | 0·18 | 0·20 | 0·18 | 0·18 | 0·21 | 0·18 | 0·16 | 0·16 |
| MgO | 2·91 | 2·97 | 2·89 | 2·78 | 3·05 | 3·06 | 4·58 | 4·54 | 3·74 | 3·56 | 3·87 | 4·17 | 5·43 | 4·50 | 2·73 | 2·38 | 2·36 |
| CaO | 7·57 | 7·39 | 7·56 | 6·94 | 7·64 | 7·50 | 10·11 | 10·24 | 9·33 | 9·14 | 9·30 | 9·66 | 10·82 | 10·10 | 7·68 | 6·57 | 6·24 |
| $Na_2O$ | 3·58 | 3·35 | 3·45 | 3·42 | 3·66 | 3·68 | 2·69 | 2·74 | 2·92 | 2·75 | 3·32 | 3·09 | 2·35 | 2·70 | 3·48 | 3·48 | 3·57 |
| $K_2O$ | 0·77 | 0·77 | 0·75 | 0·80 | 0·72 | 0·72 | 0·47 | 0·35 | 0·77 | 0·72 | 0·62 | 0·52 | 0·57 | 0·47 | 0·78 | 0·80 | 1·01 |
| $P_2O_5$ | 0·15 | 0·14 | 0·15 | 0·14 | 0·14 | 0·15 | 0·14 | 0·16 | 0·14 | 0·15 | 0·10 | 0·13 | 0·10 | 0·15 | 0·14 | 0·14 | 0·14 |
| LOI | −0·21 | −0·06 | −0·09 | 0·59 | −0·17 | −0·13 | −0·21 | −0·08 | 0·03 | −0·19 | −0·21 | −0·15 | −0·17 | −0·08 | 0·01 | 0·11 | 0·28 |
| Total | 100·51 | 100·24 | 99·97 | 99·60 | 100·36 | 99·57 | 100·19 | 99·96 | 99·51 | 99·66 | 100·00 | 99·63 | 99·87 | 99·87 | 100·07 | 100·80 | 100·31 |
| Ba | 227 | 226 | 238 | 260 | 234 | 216 | 135 | 127 | 127 | 163 | 154 | 114 | 183 | 139 | 193 | 274 | 273 |
| Rb | 15 | 16 | 16 | 17 | 16 | 11 | 10 | 5 | 14 | 14 | 13 | 11 | 8 | 10 | 19 | 19 | 19 |
| Sr | 260 | 253 | 280 | 266 | 277 | 284 | 275 | 284 | 278 | 263 | 265 | 261 | 362 | 280 | 268 | 254 | 244 |
| Zr | 100 | 92 | 101 | 121 | 104 | 101 | 64 | 70 | 73 | 84 | 63 | 65 | 55 | 69 | 89 | 111 | 109 |
| Y | 22 | 23 | 24 | 24 | 24 | 29 | 23 | 24 | 23 | 26 | 31 | 22 | 17 | 25 | 21 | 21 | 20 |
| Ni | 2 | n.d. | <2 | 4 | 2 | 3 | n.d. | 2 | 7 | 3 | 6 | 4 | 7 | <2 | 2 | 3 | n.d. |
| Cr | 14 | n.d. | 13 | n.d. | n.d. | 4 | n.d. | 16 | <2 | 7 | <2 | 6 | 32 | 31 | <2 | n.d. | n.d. |
| V | 108 | n.d. | 109 | n.d. | n.d. | 113 | n.d. | 196 | 142 | 137 | 154 | 171 | 268 | 206 | 111 | n.d. | n.d. |
| Sc | 19 | 35 | 21 | 17 | 17 | 21 | 45 | 26 | 21 | 20 | 19 | 23 | 38 | 31 | 15 | 31 | 30 |

Detection limits for Ni and Cr are about 2 ppm. MI, mafic inclusion; n.d., not determined. The basaltic lava sample, MMON32, is from the inactive South Soufriere Hills centre.

(2–5 wt %), titanomagnetite (2–4 wt %) and quartz (<0·5 wt %). Clinopyroxene (<0·5 wt %) occurs only as microphenocrysts. Apatite and ilmenite occur in trace amounts. The groundmass (<100 μm) mineralogy is similar except that amphibole is absent. Groundmass glass is high-Si rhyolite (76–79 wt % $SiO_2$). Glass proportions vary between about 5 and 25 wt %, depending on the late-stage history of individual samples. During periods of high extrusion rate, samples tend to be more glassy (up to 25 wt %) than those erupted when extrusion rates are relatively low. In the latter case, silica minerals (predominantly cristobalite) form a significant proportion of the rock (up to about 15 wt %), occurring as vesicle infills and as minute patches (<3 μm) in the groundmass, and glass proportions are reduced accordingly, as a result of late-stage microlite growth and devitrification of glass, presumably within the lava dome (Baxter *et al.*, 1999).

## Plagioclase

Plagioclase ranges in size from small (<10 μm) microlites to large phenocrysts (up to about 5 mm). Four main plagioclase populations are distinguished on the basis of composition, zoning patterns and textures (Figs 3 and 4, Table 2):

Type 1: sodic phenocrysts typically vary between $An_{48}$ and $An_{58}$, often with small-amplitude oscillatory zoning up to about $An_{64}$ (Fig. 4a). Some phenocrysts have larger amplitude patchy zoning, ranging up to about $An_{80}$.

Type 2: reverse zoned large sodic phenocrysts (Fig. 4a and b) and microphenocrysts have oscillatory zoned cores, similar ($An_{48–58}$) to the Type 1 crystals, with rims (30–150 μm) typically between $An_{65}$ and $An_{80}$. Many reverse zoned crystals remain calcic out to the edge of the grain but some have narrow (5–20 μm) more sodic rims ($\sim An_{55–65}$). Some reverse zoned crystals have outer rims with continuous normal zoning.

Type 3: reverse zoned dusty sieve-textured crystals (Fig. 4c–e) have clear oscillatory zoned sodic cores ($An_{48–58}$), similar to Type 1 and 2 crystals, with sieve-textured calcic mantles ($An_{70–88}$). Many crystals have a clear, highly calcic rim (30–200 μm), similar in composition to the sieve-textured areas. Rim zonation patterns are similar to those of the Type 2 crystals. Many crystals remain highly calcic to the outer rims but some have narrow (5–20 μm) more sodic outer rims ($\sim An_{55–65}$) on the calcic rims. Other crystals have outer rims with continuous normal zoning. The sieve-textures consist of an intimate network of calcic plagioclase (1–20 μm) and minute (<1 μm) glass patches. Boundaries between sodic cores and sieve-textured regions are irregular and truncate small-amplitude oscillatory zones in the sodic cores. The sieve-textured regions are commonly located near the outer part of the crystal but some crystals are sieve-textured throughout, with small remnant sodic patches.

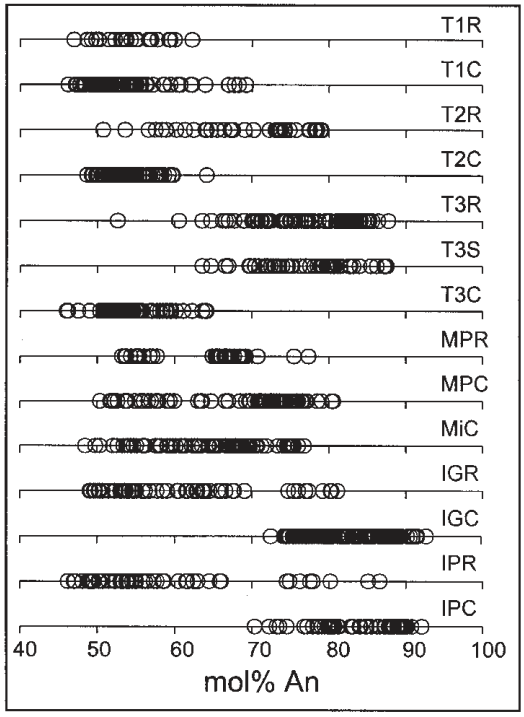


**Fig. 3.** Representative compositions of the different plagioclase populations in mol % An. R, rim; C, core; T1, T2 and T3, the three main types of phenocryst in the andesite; T3S, sieve-textured areas; MP, microphenocryst; Mi, microlite; IG and IP, inclusion groundmass and phenocryst, respectively.

Type 4: very rare highly calcic, normally zoned, clear crystals have cores between $An_{89}$ and $An_{93}$, and rims between $An_{53}$ and $An_{81}$.

The distinction between the two classes of reverse zoned crystals (Type 2 and 3) is somewhat gradational, as some crystals classified as Type 2 have very narrow regions with poorly developed or partial sieve-textures (Fig. 4b). However, the reverse zoned regions of Type 3 crystals commonly extend to more calcic compositions than in the Type 2 crystals. Together, Type 2 and 3 crystals typically form between 30 and 50% of the total plagioclase phenocryst population. Most reverse zoned crystals do not have extensive sodic overgrowths at the rims.

Plagioclase microphenocrysts have a similar range in composition to the larger phenocrysts. Calcic microphenocrysts have cores in the range $An_{65–85}$. Some calcic microphenocrysts have narrow (5–10 μm) sodic rims, $An_{55–60}$. Sodic microphenocrysts have similar compositions ($An_{48–58}$) to the sodic phenocrysts. Groundmass plagioclase microlites range widely between about $An_{48}$ and $An_{75}$ but individual microlites generally have a narrow ($\pm An_5$) compositional range. Some are unzoned and

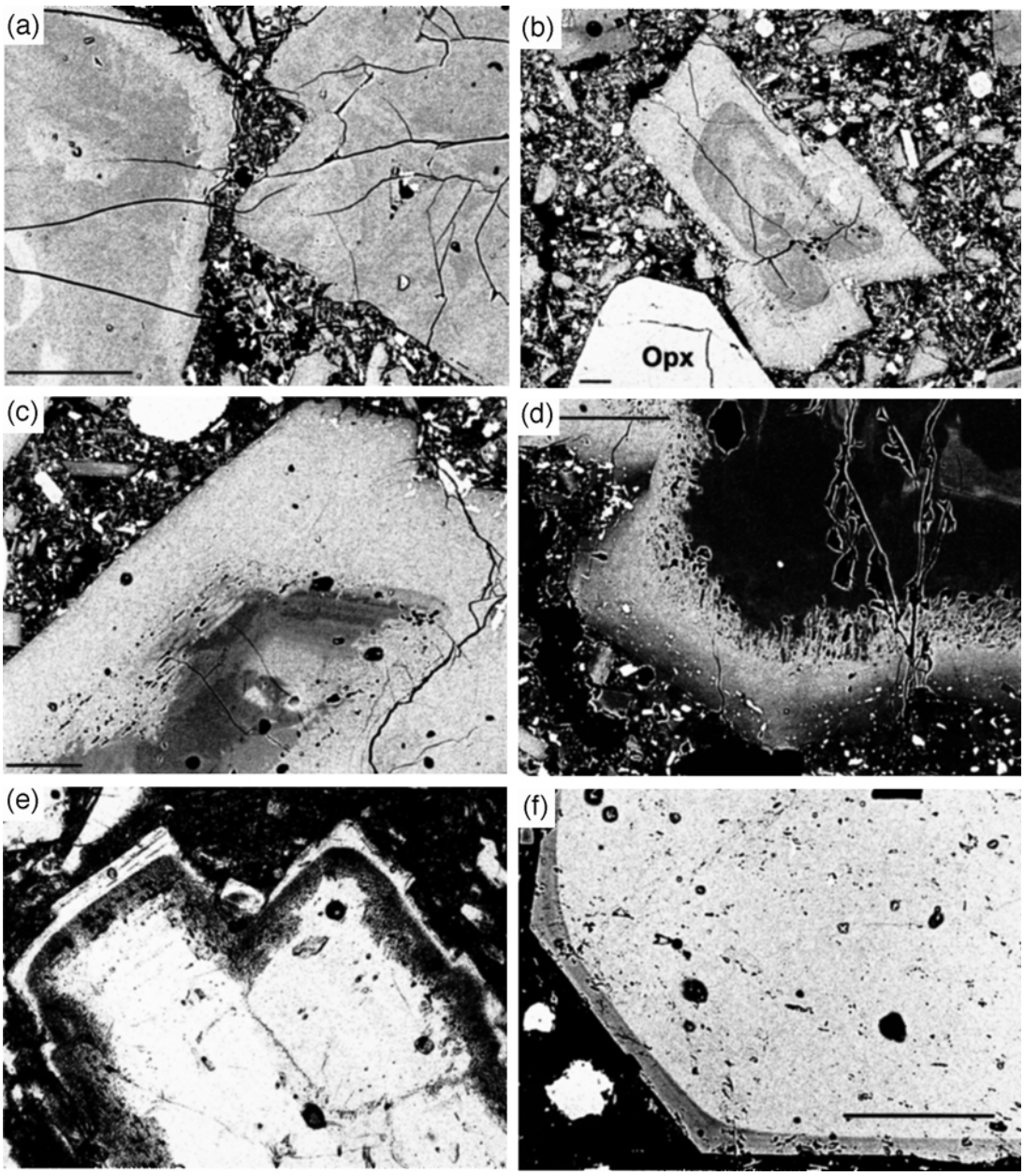


**Fig. 4.** Back-scattered electronmicrographs and photomicrographs of plagioclase and orthopyroxene phenocryst textures. Scale bar in all electronmicrographs represents 100 μm. (a) Coexisting Type 1 and Type 2 plagioclase phenocrysts. The Type 2 crystal on the left has a dark sodic core and a light calcic rim. (b) Reverse zoned plagioclase phenocryst with wide calcic rim and poorly developed sieve texture. It should be noted that most plagioclase microphenocrysts are relatively calcic, similar to the rim of the phenocryst, but that some are more sodic. (c) Reverse zoned Type 3 sieve-textured plagioclase phenocryst with wide calcic rim. (d) Reverse zoned Type 3 sieve-textured plagioclase phenocryst with calcic rim, which becomes more sodic towards the edge of the crystal. (e) Photomicrograph (crossed polars) of sieve-textured plagioclase phenocryst. Field of view is 2·7 mm. (f) Reverse zoned orthopyroxene phenocryst. The magnesian rim is darker than the more Fe-rich core.

others are reverse zoned. Small euhedral plagioclase crystals (~30–300 μm) also occur as inclusions in amphibole. Many are similar in composition to the sodic phenocrysts and the overall range is about $An_{48–77}$. Plagioclase also occurs as intergrowths with pyroxene and titanomagnetite, formed by breakdown of amphibole (see below).

## Pyroxene

Orthopyroxene ranges in size from small microlites (<10 μm) up to about 5 mm, occurring as individual phenocrysts, in crystal clots and as inclusions in amphibole. Three main phenocryst populations can be defined on the basis of rim composition (Fig. 5, Table 3):

*Table 2: Representative average plagioclase analyses*

| | Andesite | | | | | | | | | | | | | Mafic inclusion | | | |
|---|---|---|---|---|---|---|---|---|---|---|---|---|---|---|---|---|---|
| | T1PhR | T1PhC | T2PhR | T2PhC | T3PhR | T3PhS | T3PhC | T4C | MPC | MPC | Gms | Gms | Gms | PhR | PhC | GmsR | GmsC |
| No. analyses: | 6 | 9 | 9 | 11 | 14 | 8 | 7 | 11 | 7 | 7 | 3 | 4 | 4 | 5 | 22 | 4 | 10 |
| $SiO_2$ | 55·53 | 55·72 | 49·72 | 54·70 | 46·92 | 48·23 | 53·92 | 44·96 | 48·61 | 55·43 | 54·92 | 52·49 | 50·20 | 55·26 | 46·17 | 51·12 | 47·17 |
| $Al_2O_3$ | 27·18 | 27·50 | 31·42 | 28·65 | 33·02 | 32·49 | 28·71 | 34·51 | 32·07 | 28·16 | 27·52 | 28·95 | 30·97 | 28·04 | 34·26 | 31·10 | 33·82 |
| $FeO^T$ | 0·32 | 0·29 | 0·63 | 0·30 | 0·51 | 0·50 | 0·25 | 0·47 | 0·58 | 0·28 | 0·66 | 0·87 | 0·65 | 0·41 | 0·50 | 0·61 | 0·55 |
| MnO | 0·00 | 0·00 | 0·02 | 0·01 | 0·00 | 0·00 | 0·00 | 0·01 | 0·01 | 0·00 | 0·07 | 0·00 | 0·00 | 0·00 | 0·01 | 0·00 | 0·01 |
| MgO | 0·01 | 0·01 | 0·09 | 0·03 | 0·05 | 0·02 | 0·00 | 0·04 | 0·06 | 0·00 | 0·03 | 0·00 | 0·00 | 0·06 | 0·07 | 0·05 | 0·06 |
| CaO | 10·37 | 10·44 | 14·88 | 11·16 | 17·01 | 16·36 | 11·50 | 18·62 | 15·78 | 10·89 | 10·80 | 12·54 | 14·54 | 11·08 | 18·25 | 14·17 | 17·30 |
| $Na_2O$ | 5·45 | 5·45 | 3·22 | 5·25 | 1·88 | 2·04 | 4·84 | 1·03 | 2·46 | 5·38 | 4·93 | 4·27 | 3·40 | 5·49 | 1·35 | 3·58 | 1·85 |
| $K_2O$ | 0·14 | 0·13 | 0·07 | 0·14 | 0·01 | 0·14 | 0·09 | 0·02 | 0·03 | 0·12 | 0·44 | 0·18 | 0·07 | 0·09 | 0·02 | 0·03 | 0·01 |
| Total | 98·99 | 99·55 | 100·07 | 100·24 | 99·40 | 99·77 | 99·30 | 99·66 | 99·60 | 100·27 | 99·39 | 99·28 | 99·82 | 100·44 | 100·63 | 100·67 | 100·77 |
| $Si^{4+}$ | 2·526 | 2·520 | 2·276 | 2·466 | 2·173 | 2·218 | 2·453 | 2·087 | 2·238 | 2·493 | 2·499 | 2·405 | 2·300 | 2·486 | 2·119 | 2·317 | 2·156 |
| $Al^{3+}$ | 1·457 | 1·466 | 1·695 | 1·522 | 1·802 | 1·761 | 1·539 | 1·888 | 1·740 | 1·493 | 1·476 | 1·564 | 1·672 | 1·487 | 1·853 | 1·661 | 1·822 |
| $Fe^{2+}$ | 0·012 | 0·011 | 0·024 | 0·011 | 0·020 | 0·019 | 0·009 | 0·018 | 0·022 | 0·010 | 0·025 | 0·033 | 0·025 | 0·015 | 0·019 | 0·023 | 0·021 |
| $Mn^{2+}$ | 0·000 | 0·000 | 0·001 | 0·000 | 0·000 | 0·000 | 0·000 | 0·000 | 0·000 | 0·000 | 0·003 | 0·000 | 0·000 | 0·000 | 0·000 | 0·000 | 0·000 |
| $Mg^{2+}$ | 0·001 | 0·000 | 0·006 | 0·002 | 0·003 | 0·002 | 0·000 | 0·003 | 0·004 | 0·000 | 0·002 | 0·000 | 0·000 | 0·004 | 0·005 | 0·003 | 0·004 |
| $Ca^{2+}$ | 0·505 | 0·506 | 0·730 | 0·539 | 0·844 | 0·806 | 0·560 | 0·926 | 0·778 | 0·525 | 0·527 | 0·616 | 0·714 | 0·534 | 0·897 | 0·688 | 0·847 |
| $Na^+$ | 0·480 | 0·478 | 0·286 | 0·459 | 0·169 | 0·182 | 0·427 | 0·092 | 0·220 | 0·469 | 0·435 | 0·379 | 0·302 | 0·479 | 0·120 | 0·314 | 0·164 |
| $K^+$ | 0·008 | 0·008 | 0·004 | 0·008 | 0·001 | 0·008 | 0·005 | 0·001 | 0·002 | 0·007 | 0·025 | 0·010 | 0·004 | 0·005 | 0·001 | 0·002 | 0·001 |
| Total | 4·990 | 4·989 | 5·022 | 5·007 | 5·011 | 4·996 | 4·994 | 5·016 | 5·003 | 4·998 | 4·993 | 5·007 | 5·017 | 5·011 | 5·015 | 5·009 | 5·015 |
| An | 0·508 | 0·510 | 0·716 | 0·536 | 0·833 | 0·809 | 0·565 | 0·908 | 0·778 | 0·524 | 0·533 | 0·613 | 0·700 | 0·524 | 0·881 | 0·685 | 0·837 |
| Ab | 0·483 | 0·482 | 0·280 | 0·456 | 0·166 | 0·182 | 0·430 | 0·091 | 0·220 | 0·469 | 0·441 | 0·377 | 0·296 | 0·471 | 0·118 | 0·313 | 0·162 |
| Or | 0·008 | 0·008 | 0·004 | 0·008 | 0·001 | 0·008 | 0·005 | 0·001 | 0·002 | 0·007 | 0·026 | 0·010 | 0·004 | 0·005 | 0·001 | 0·002 | 0·001 |
| An(max) | 0·525 | 0·577 | 0·789 | 0·587 | 0·852 | 0·828 | 0·597 | 0·927 | 0·794 | 0·539 | 0·586 | 0·662 | 0·725 | 0·567 | 0·921 | 0·747 | 0·891 |
| An(min) | 0·502 | 0·482 | 0·647 | 0·486 | 0·821 | 0·785 | 0·542 | 0·889 | 0·758 | 0·504 | 0·497 | 0·560 | 0·639 | 0·469 | 0·814 | 0·638 | 0·796 |

Each column is the average composition of a single crystal. The number of analyses and maximum and minimum An content of the crystal are also shown. T1, T2, T3 and T4 are the different types (see text); Ph, phenocryst; C, core; R, rim; S, sieve-textured; MP, microphenocryst; Gms, groundmass.

(1) Unzoned crystals have narrow ranges in composition, with En and Wo contents typically in the range 57–61 and 1·8–2·3, respectively.

(2) Reverse zoned crystals have similar cores to the unzoned crystals but the rims have higher En (62–73) and Wo (2·2–3·7) (Figs 4f and 5), with a much smaller intra-grain than inter-grain variation (Table 3). Orthopyroxene in samples erupted during the early stages of the current eruption has very narrow (<5 μm) reverse zoned rims but all samples erupted since May 1996 contain orthopyroxene with well-developed reverse zoned rims (10–25 μm). No consistent variation has been observed in the width or composition of the reverse rims since May 1996.

(3) Crystals with clinopyroxene rims (~10–30 μm) have similar core compositions to the Type 1 and 2 crystals.

The three populations coexist in most samples. In addition, rare crystals with similar En but much lower Wo, ranging between 1·2 and 1·5, occur in a few samples (Table 3). These low-Wo crystals are more abundant in the older Soufriere Hills andesites.

Orthopyroxene occurs as groundmass microlites and as reaction products formed by breakdown of amphibole (see below). En typically ranges between 63 and 70 but Wo contents vary more, ranging from about $Wo_3$ to $Wo_5$, and grading into pigeonite (Fig. 5). The variations in Wo content occur as patches or discrete sectors within individual grains and some orthopyroxene microlites have pigeonite rims. Groundmass microlites and crystals in coarse amphibole breakdown textures are similar in composition but orthopyroxene in very fine-grained amphibole breakdown textures has slightly lower En, ranging between 63 and 67.

Clinopyroxene occurs as microphenocrysts (<300 μm) and microlites, as rims on orthopyroxene and as breakdown products of amphibole. Patchy and sector zoning are common with complex variations in Al, Ti, Mg, Fe, Ca and Si. En is in the range 66–73 and Wo generally ranges from 32 to 43, with an overall range of about 20–46, grading into pigeonite at the lower end of the range. Clinopyroxene in the fine-scale amphibole breakdown textures has slightly lower average En, between about 65 and 70.

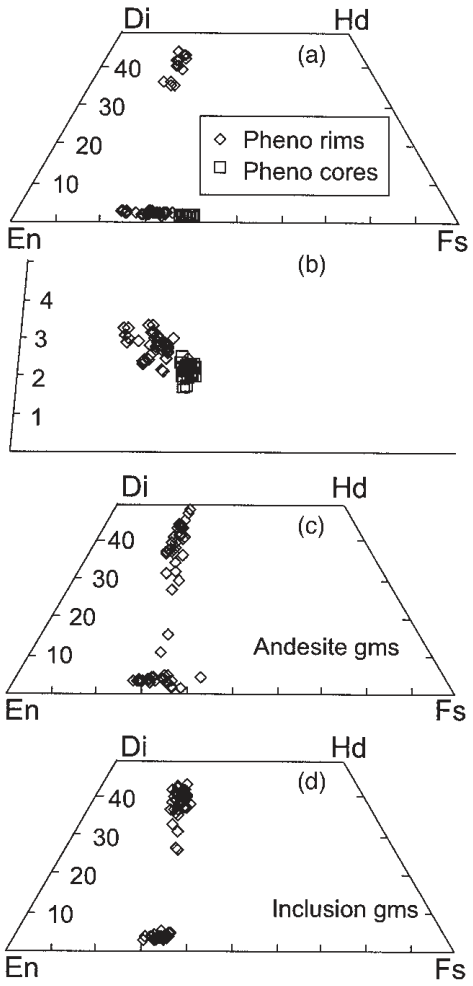


**Fig. 5.** Representative pyroxene compositions plotted as mol % of the simple quadrilateral components. (a) Compositions of orthopyroxene phenocryst cores and rims and of clinopyroxene rims on orthopyroxene phenocrysts in the recent andesite. (b) Expanded version of (a) to show the differences in Wo content of the orthopyroxene rims compared with the cores. (c) Compositions of groundmass pyroxenes, including clinopyroxene microphenocrysts. (d) Compositions of mafic inclusion groundmass pyroxenes.

## Amphibole

Euhedral to anhedral amphibole phenocrysts range between about 0·5 mm and 1 cm in size, occurring as individual crystals and in clots with plagioclase, orthopyroxene and titanomagnetite. The same minerals are abundant as inclusions in amphibole. There is considerable variation in the sizes, proportions and distributions of inclusions from one amphibole crystal to another. All are calcic amphiboles (Table 4), magnesiohornblendes in the terminology of Leake *et al.* (1997). $Al_2O_3$ contents are low (Table 4, Fig. 6), typically between 6 and 8%, extending up to 9% in a few crystals. Some crystals have rims with slightly lower $Fe^T/Mg$ than the cores (Table 4). Small inclusions of amphibole occur in the calcic rims of some sieve-textured plagioclase. These are aluminous (up to 14 wt % $Al_2O_3$), similar in composition to amphibole in the mafic inclusions, discussed below.

Some samples, particularly explosive pumice ejecta, contain predominantly pristine euhedral or slightly rounded amphibole, with light to dark green pleochroism. In slowly erupted dome samples, many crystals have reaction

*Table 3: Representative average pyroxene analyses*

| | Current andesite | | | | | | | | | | | Current mafic inclusion | | | | 18 ka andesite | |
|---|---|---|---|---|---|---|---|---|---|---|---|---|---|---|---|---|---|
| | PhR | PhC | PhR | PhC | PhC | MP | MP | Gms | Gms | Gms | Gms | Gms | Gms | Gms | Gms | Ph C | Ph C |
| No. analyses: | 7 | 5 | 9 | 5 | 11 | 7 | 6 | 5 | 3 | 6 | 7 | 4 | 3 | 5 | 5 | 4 | 5 |
| $SiO_2$ | 53·40 | 52·48 | 53·94 | 52·84 | 52·16 | 52·17 | 52·39 | 54·33 | 53·80 | 52·64 | 51·56 | 51·07 | 51·32 | 52·70 | 53·66 | 52·31 | 52·73 |
| $TiO_2$ | 0·14 | 0·06 | 0·11 | 0·07 | 0·07 | 0·23 | 0·29 | 0·11 | 0·30 | 0·32 | 0·40 | 0·57 | 0·47 | 0·26 | 0·27 | 0·06 | 0·10 |
| $Al_2O_3$ | 1·12 | 0·63 | 1·15 | 0·52 | 0·64 | 1·15 | 1·18 | 0·71 | 1·01 | 1·62 | 2·74 | 2·28 | 2·23 | 1·66 | 0·77 | 0·41 | 0·61 |
| $FeO^T$ | 19·56 | 23·81 | 16·96 | 23·62 | 24·33 | 9·96 | 10·54 | 17·37 | 20·47 | 11·10 | 10·08 | 12·19 | 13·73 | 22·12 | 21·32 | 25·04 | 24·11 |
| MnO | 0·92 | 1·75 | 0·61 | 1·45 | 1·59 | 0·69 | 0·75 | 0·74 | 0·97 | 0·65 | 0·51 | 0·70 | 0·81 | 1·18 | 0·76 | 1·73 | 1·63 |
| MgO | 22·88 | 19·67 | 26·09 | 21·25 | 20·14 | 14·41 | 14·83 | 24·46 | 19·60 | 15·74 | 14·63 | 13·78 | 13·81 | 21·31 | 22·45 | 20·48 | 20·75 |
| CaO | 1·43 | 1·03 | 1·52 | 1·00 | 0·64 | 21·41 | 20·24 | 1·58 | 2·05 | 18·94 | 20·11 | 19·63 | 17·78 | 1·69 | 1·76 | 0·62 | 0·96 |
| $Na_2O$ | | | | | | 0·25 | 0·22 | | | 0·18 | 0·20 | 0·28 | 0·27 | | | | |
| Total | 99·45 | 99·41 | 100·40 | 100·74 | 99·58 | 100·27 | 100·44 | 99·30 | 98·20 | 101·17 | 100·22 | 100·49 | 100·41 | 100·91 | 100·98 | 100·64 | 100·89 |
| $Si^{4+}$ | 1·980 | 1·993 | 1·957 | 1·976 | 1·981 | 1·952 | 1·955 | 1·994 | 2·025 | 1·945 | 1·921 | 1·919 | 1·932 | 1·953 | 1·976 | 1·973 | 1·974 |
| $Ti^{4+}$ | 0·004 | 0·002 | 0·003 | 0·002 | 0·002 | 0·007 | 0·008 | 0·003 | 0·009 | 0·009 | 0·011 | 0·016 | 0·013 | 0·007 | 0·008 | 0·002 | 0·003 |
| $Al^{3+}$ | 0·049 | 0·028 | 0·049 | 0·023 | 0·029 | 0·051 | 0·052 | 0·031 | 0·045 | 0·070 | 0·121 | 0·101 | 0·099 | 0·073 | 0·033 | 0·018 | 0·027 |
| $Fe^{2+}$ | 0·607 | 0·756 | 0·515 | 0·739 | 0·773 | 0·312 | 0·329 | 0·533 | 0·645 | 0·343 | 0·314 | 0·383 | 0·432 | 0·686 | 0·656 | 0·790 | 0·755 |
| $Mn^{2+}$ | 0·029 | 0·056 | 0·019 | 0·046 | 0·051 | 0·022 | 0·024 | 0·023 | 0·031 | 0·020 | 0·016 | 0·022 | 0·026 | 0·037 | 0·024 | 0·055 | 0·052 |
| $Mg^{2+}$ | 1·265 | 1·114 | 1·411 | 1·185 | 1·140 | 0·804 | 0·825 | 1·338 | 1·099 | 0·867 | 0·813 | 0·772 | 0·775 | 1·178 | 1·233 | 1·151 | 1·158 |
| $Ca^{2+}$ | 0·057 | 0·042 | 0·059 | 0·040 | 0·026 | 0·858 | 0·809 | 0·062 | 0·083 | 0·750 | 0·803 | 0·790 | 0·717 | 0·067 | 0·069 | 0·025 | 0·038 |
| $Na^{+}$ | | | | | | 0·018 | 0·016 | | | 0·013 | 0·015 | 0·020 | 0·020 | 0·003 | 0·002 | | |
| Total | 3·991 | 3·991 | 4·014 | 4·010 | 4·002 | 4·023 | 4·018 | 3·985 | 3·936 | 4·017 | 4·014 | 4·023 | 4·014 | 4·003 | 4·001 | 4·014 | 4·007 |
| En | 0·656 | 0·583 | 0·711 | 0·603 | 0·588 | 0·407 | 0·420 | 0·692 | 0·602 | 0·442 | 0·421 | 0·397 | 0·403 | 0·610 | 0·629 | 0·586 | 0·593 |
| Fs | 0·315 | 0·395 | 0·259 | 0·376 | 0·399 | 0·158 | 0·168 | 0·276 | 0·353 | 0·175 | 0·163 | 0·197 | 0·225 | 0·355 | 0·335 | 0·402 | 0·387 |
| Wo | 0·029 | 0·022 | 0·030 | 0·020 | 0·013 | 0·435 | 0·412 | 0·032 | 0·045 | 0·383 | 0·416 | 0·406 | 0·373 | 0·035 | 0·035 | 0·013 | 0·020 |
| En(max) | 0·662 | 0·586 | 0·730 | 0·606 | 0·592 | 0·421 | 0·432 | 0·705 | 0·633 | 0·450 | 0·451 | 0·408 | 0·410 | 0·616 | 0·635 | 0·590 | 0·600 |
| En(min) | 0·651 | 0·578 | 0·675 | 0·602 | 0·584 | 0·393 | 0·412 | 0·673 | 0·550 | 0·432 | 0·399 | 0·392 | 0·399 | 0·604 | 0·624 | 0·582 | 0·587 |
| Wo(max) | 0·031 | 0·023 | 0·033 | 0·022 | 0·015 | 0·448 | 0·426 | 0·034 | 0·046 | 0·398 | 0·442 | 0·414 | 0·385 | 0·035 | 0·037 | 0·013 | 0·021 |
| Wo(min) | 0·028 | 0·021 | 0·026 | 0·019 | 0·012 | 0·417 | 0·393 | 0·030 | 0·043 | 0·372 | 0·383 | 0·394 | 0·356 | 0·034 | 0·033 | 0·012 | 0·019 |
| *T* (°C) | 988 | 870 | 1027 | 855 | 749 | | | | | | | 1049 | 1085 | 1024 | 1034 | 748 | 849 |

Each column represents the average of a single crystal. The number of analyses and maximum and minimum En and Wo content of the crystal are also shown. Abbreviations as in Table 2. The calculated QUILF temperatures (1·5 kbar) are given in the last row where appropriate.

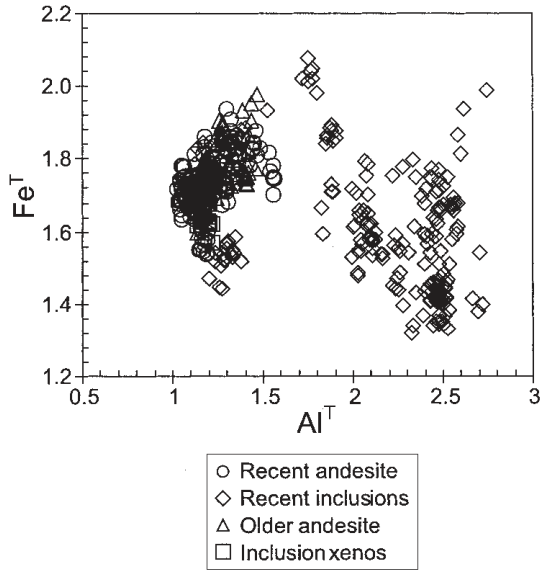


**Fig. 6.** Representative amphibole compositions plotted as molar $Fe^T$ against $Al^T$ calculated for 23 oxygens. Amphibole in the mafic inclusions is mostly significantly more aluminous than that in the andesite but some crystals in the inclusions have compositions that overlap with those in the andesite. Xenocrysts in mafic inclusions and phenocrysts in older andesites are similar to phenocrysts in the recent andesite.

textures (Devine *et al.*, 1998*a*). Three textures can be defined (Fig. 7):

Type 1: fine-grained (~5–30 μm) intergrowths of clinopyroxene, orthopyroxene, pigeonite, plagioclase and titanomagnetite occur as rims and along the cleavages of many crystals (Fig. 7a and b).

Type 2: crystals with a coarser-grained (~30–200 μm) intergrowth of the same phases as in Type 1 occur in most samples (Fig. 7c and d). In many cases, the clinopyroxene forms an optically continuous patchwork texture replacing the original amphibole (Fig. 7c). The extent of the texture is variable but many crystals are often almost completely pseudomorphed with small patches of remnant amphibole in the cores.

Type 3: opaque replacement [opacite, see Garcia & Jacobson (1979)] occurs at the rims and along cleavages of many crystals (Fig. 7e). In some slowly erupted samples, the amphiboles are completely pseudomorphed by opacite. The opacite texture consists of a very fine-grained intergrowth (1–10 μm) of the same phases as in Types 1 and 2, but titanomagnetite predominates over the other mafic minerals.

Many samples contain crystals with all three reaction textures. The Type 3 texture appears to form at a late stage by oxidation within the lava dome. The Type 1 texture is believed to form during ascent (Devine *et al.*, 1998*a*), as amphibole becomes unstable at pressures less than ~1·5 kbar and breaks down to form an anhydrous assemblage. The extent of the reaction rims can be used to estimate magma ascent rates (Rutherford & Hill, 1993; Devine *et al.*, 1998*a*). Some crystals have both Type 1 and Type 3 textures, as a result of late-stage oxidation of unreacted amphibole. The coarse Type 2 texture may form on crystals that spend long periods in the conduit, outside the amphibole stability field, or may be related to heating of the andesite by intruding mafic magma (see below).

### Fe–Ti oxides

Titanomagnetite occurs as individual microphenocryst and microlites, as inclusions in phenocrysts and in intergrowths formed by amphibole breakdown. In slowly erupted lava samples, titanomagnetite has very fine-scale lamellar exsolution textures and is heterogeneous in composition. Crystals formed by breakdown of amphibole are also very heterogeneous. In pumice and rapidly erupted dome samples, individual crystals are more homogeneous in composition, although there is still significant variation between grains in individual samples (Table 5). Ilmenite is present in very minor amounts, probably much less than 1% of the total Fe–Ti oxide population.

### Quartz

Quartz occurs as rounded individual crystals (0·5–2 mm), typically one or two per thin section. Some crystals have reaction rims of clinopyroxene. Quartz does not occur intergrown with other phenocrysts. Rhyolitic melt inclusions are common in quartz.

## MAFIC INCLUSION PETROLOGY

Mafic inclusions are a ubiquitous but minor component of the andesite, forming <1 wt % of the lava. The inclusions range in size from about 40 cm to about 1 mm in diameter (Fig. 8a and b). The inclusions most commonly have ellipsoidal shapes but some are angular (Fig. 8a). They have sharply defined smooth or crenulate contacts with the andesite host (Fig. 8b) and some have chilled margins, defined by a decrease in groundmass grain size at the inclusion–host contact.

Most inclusions are phenocryst poor (~1–5%) and contain phenocrysts of plagioclase only. The inclusions have diktytaxitic quench-textured groundmass (see Bacon, 1986) consisting of randomly oriented, interlocking, elongate or acicular crystals (Fig. 8c–e). The groundmass framework consists of plagioclase ± clinopyroxene ± orthopyroxene ± amphibole, titanomagnetite, patches of interstitial rhyolitic glass and abundant interstitial voids, in some cases infilled

*Table 4: Representative average amphibole analyses*

| | Current andesite | | | | Current mafic inclusions | | | | | | | Andesite | |
|---|---|---|---|---|---|---|---|---|---|---|---|---|---|
| | | | | | | | | | | | | ~3·7 ka | ~18 ka |
| | C | C | C | Pl Inc | R | C | C | C | C | C | C | C | C |
| No. analyses: | 12 | 9 | 9 | 5 | 4 | 7 | 4 | 5 | 6 | 3 | 3 | 4 | 5 |
| $SiO_2$ | 48·61 | 48·12 | 46·51 | 42·44 | 42·76 | 43·10 | 41·86 | 41·68 | 40·76 | 41·20 | 47·10 | 46·81 | 48·71 |
| $TiO_2$ | 1·28 | 1·42 | 1·74 | 1·98 | 1·77 | 1·72 | 1·78 | 1·68 | 1·94 | 1·78 | 1·65 | 1·60 | 1·50 |
| $Al_2O_3$ | 6·20 | 6·64 | 7·51 | 13·12 | 12·23 | 12·03 | 13·34 | 14·07 | 14·37 | 14·01 | 7·46 | 7·65 | 6·96 |
| $FeO^T$ | 14·37 | 14·12 | 14·01 | 12·91 | 13·35 | 12·84 | 12·95 | 12·50 | 14·01 | 12·46 | 12·52 | 14·41 | 13·79 |
| MnO | 0·56 | 0·53 | 0·53 | 0·25 | 0·24 | 0·25 | 0·19 | 0·21 | 0·29 | 0·21 | 0·39 | 0·55 | 0·39 |
| MgO | 14·02 | 14·47 | 13·84 | 13·64 | 13·40 | 14·05 | 13·44 | 13·40 | 12·16 | 12·73 | 14·36 | 14·02 | 14·67 |
| CaO | 10·97 | 11·15 | 11·25 | 11·50 | 11·66 | 11·55 | 11·82 | 11·83 | 11·20 | 11·54 | 11·36 | 10·92 | 11·33 |
| $Na_2O$ | 1·11 | 1·27 | 1·44 | 2·15 | 2·21 | 2·23 | 2·35 | 2·38 | 2·16 | 2·22 | 1·77 | 1·37 | 1·31 |
| $K_2O$ | 0·17 | 0·17 | 0·19 | 0·21 | 0·24 | 0·27 | 0·22 | 0·18 | 0·21 | 0·19 | 0·18 | 0·19 | 0·19 |
| Total | 97·30 | 97·89 | 97·02 | 98·21 | 97·88 | 98·08 | 97·96 | 97·96 | 97·09 | 96·34 | 96·81 | 97·51 | 98·84 |
| $Si^{4+}$ | 7·073 | 6·954 | 6·797 | 6·105 | 6·202 | 6·215 | 6·061 | 6·022 | 5·965 | 6·058 | 6·870 | 6·792 | 6·948 |
| $Ti^{4+}$ | 0·140 | 0·155 | 0·192 | 0·215 | 0·193 | 0·186 | 0·194 | 0·183 | 0·214 | 0·197 | 0·182 | 0·175 | 0·161 |
| $Al^{IV}$ | 0·927 | 1·046 | 1·203 | 1·895 | 1·798 | 1·785 | 1·940 | 1·978 | 2·035 | 1·942 | 1·130 | 1·208 | 1·052 |
| $Al^{VI}$ | 0·136 | 0·085 | 0·090 | 0·329 | 0·292 | 0·258 | 0·337 | 0·419 | 0·444 | 0·486 | 0·153 | 0·100 | 0·119 |
| $Fe^{3+}$ | 0·476 | 0·560 | 0·615 | 0·845 | 0·758 | 0·813 | 0·798 | 0·777 | 0·878 | 0·694 | 0·463 | 0·695 | 0·573 |
| $Fe^{2+}$ | 1·273 | 1·146 | 1·097 | 0·708 | 0·860 | 0·735 | 0·769 | 0·735 | 0·837 | 0·838 | 1·064 | 1·054 | 1·072 |
| $Mn^{2+}$ | 0·069 | 0·065 | 0·065 | 0·031 | 0·029 | 0·030 | 0·023 | 0·025 | 0·035 | 0·025 | 0·049 | 0·068 | 0·047 |
| $Mg^{2+}$ | 3·041 | 3·117 | 3·015 | 2·926 | 2·898 | 3·020 | 2·901 | 2·885 | 2·653 | 2·791 | 3·122 | 3·034 | 3·119 |
| $Ca^{2+}$ | 1·710 | 1·726 | 1·762 | 1·772 | 1·811 | 1·784 | 1·834 | 1·831 | 1·757 | 1·818 | 1·775 | 1·698 | 1·732 |
| $Na^{M4}$ | 0·155 | 0·147 | 0·164 | 0·174 | 0·154 | 0·168 | 0·142 | 0·143 | 0·183 | 0·150 | 0·192 | 0·178 | 0·178 |
| $Na^{A}$ | 0·158 | 0·208 | 0·243 | 0·426 | 0·466 | 0·455 | 0·517 | 0·524 | 0·429 | 0·482 | 0·310 | 0·207 | 0·183 |
| $K^+$ | 0·032 | 0·031 | 0·035 | 0·039 | 0·045 | 0·049 | 0·040 | 0·033 | 0·039 | 0·036 | 0·033 | 0·035 | 0·035 |
| Total | 15·190 | 15·239 | 15·278 | 15·465 | 15·511 | 15·503 | 15·556 | 15·557 | 15·468 | 15·518 | 15·343 | 15·241 | 15·218 |

Each column is the average of a single crystal. Cation proportions calculated for 23 oxygens using the method of Holland & Blundy (1994). Pl Inc, amphibole inclusion in a sieve-textured plagioclase.

by vapour-phase silica. Larger inclusions tend to have coarser-grained groundmass than small inclusions, and framework plagioclase crystals have more equant shapes (Fig. 8c and d). Amphibole is the most abundant mafic phase in larger inclusions but in small inclusions, less than a few centimetres in size, pyroxene predominates.

Large crystals of plagioclase, amphibole, orthopyroxene and quartz in the inclusions are identified on the basis of composition and/or morphology as xenocrysts derived from the andesite. In some cases, large plagioclase phenocrysts from the andesite are partially incorporated into mafic inclusions (Fig. 8e and f). The xenocrysts are very commonly resorbed, with reaction textures that are similar to but more extensive than reaction textures on phenocrysts in the andesite. Plagioclase xenocrysts have strongly developed sieve textures, which may permeate the entire crystal, in contrast to similar Type 3 crystals in the andesite, which have experienced only partial resorption. Large amphibole xenocrysts typically have extensive fine-grained reaction textures, which consist of minor olivine ($\sim Fo_{60}$) in addition to pyroxene, plagioclase and titanomagnetite (Fig. 7f). Quartz xenocrysts have wide rims of clinopyroxene.

The framework plagioclase is calcic, typically ranging from $An_{70}$ to $An_{89}$ in the cores (Fig. 3, Table 2). Rims are often relatively sodic, $An_{47–58}$. Larger plagioclase crystals range to more calcic compositions than the framework plagioclase, up to $An_{93}$. Dusty sieve-textured crystals are compositionally similar to those in the andesite but commonly have wide (up to $\sim 100$ μm) sodic ($An_{47–58}$) overgrowths on the calcic rims, in contrast to

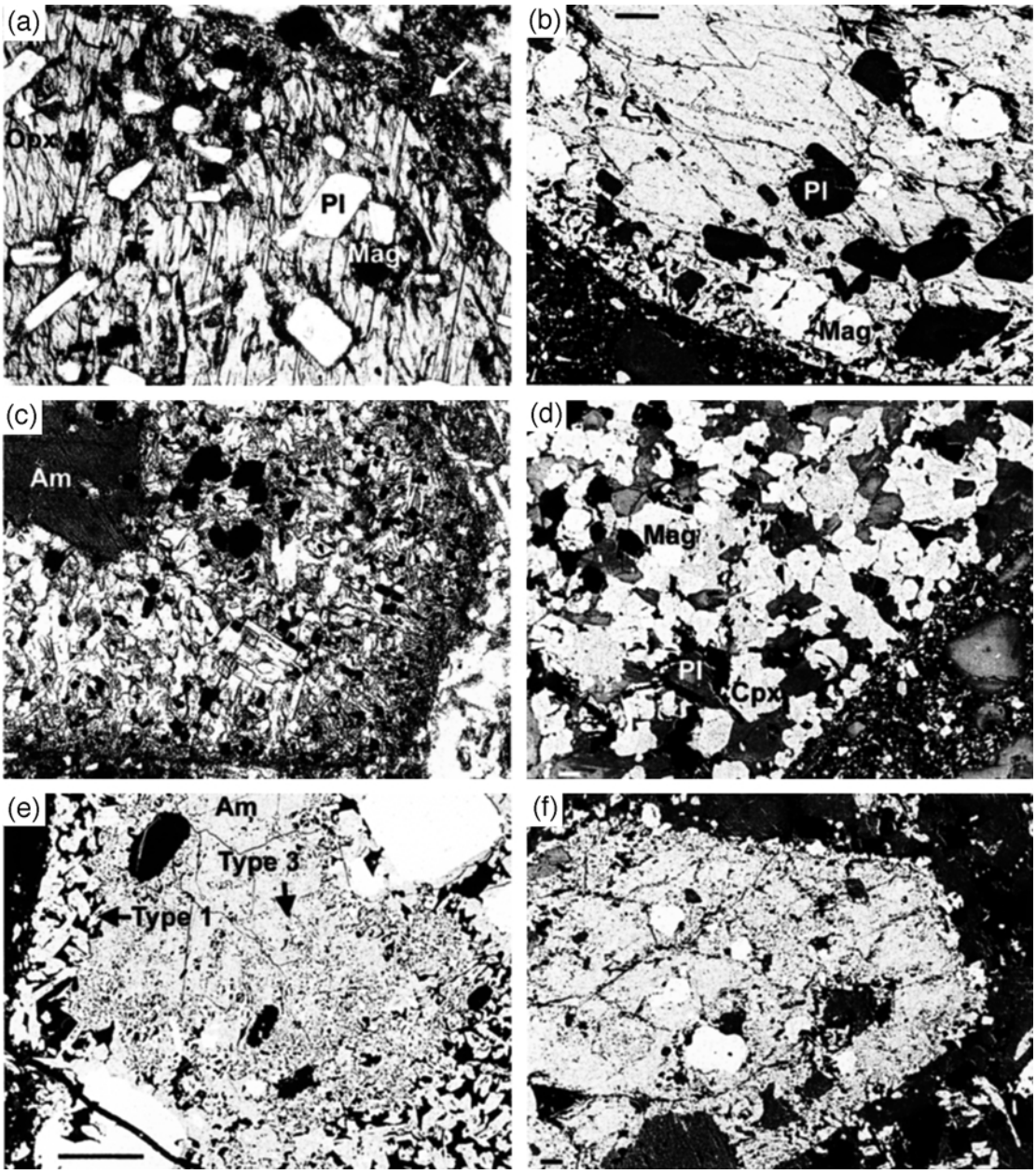


**Fig. 7.** Amphibole textures. Scale bar in all electronmicrographs represents 100 μm. Field of view in all photomicrographs is 2·7 mm. (a) Photomicrograph (plane-polarized light; PPL) of large amphibole phenocryst with Type 1 fine-grained reaction rim at top right (arrowed). (b) Electronmicrograph of large amphibole phenocryst with Type 1 reaction rim. Scale bar at top left. (c) Photomicrograph (PPL) of Type 2 reaction texture. The crystal has been pseudomorphed by a coarse-grained intergrowth, consisting of optically continuous clinopyroxene, plagioclase, orthopyroxene and titanomagnetite. Remnant amphibole is visible at the top left. (d) Electronmicrograph of coarse-grained amphibole pseudomorph similar to (c). Scale bar at bottom left. (e) Electronmicrograph of amphibole with very fine-grained Type 3 (opacite) texture in the core and Type 1 reaction rim. Large areas of original amphibole remain in the core. (f) Electronmicrograph of amphibole xenocryst in mafic inclusion with fine-grained reaction texture, consisting of olivine in addition to pyroxenes, plagioclase and titanomagnetite. Scale bar at bottom left.

sieve-textured crystals in the andesite, which typically have very narrow (5–20 μm) or no sodic rims.

The groundmass framework amphibole in the mafic inclusions is highly aluminous, mostly in the range 12–14·5% $Al_2O_3$ (Table 4, Fig. 6), much higher than amphibole in the andesite (typically 6–8% $Al_2O_3$). Crystals are often heterogeneous with patchy zoning, the different segments showing complementary variations in Al and

*Table 5: Representative average titanomagnetite analyses*

| | Andesite | | | | Mafic inclusion | | | |
|---|---|---|---|---|---|---|---|---|
| No. analyses: | 9 | 6 | 8 | 5 | 8 | 8 | 2 | 7 |
| $SiO_2$ | 0·10 | 0·26 | 0·11 | 0·06 | 0·19 | 0·37 | 0·25 | 0·23 |
| $TiO_2$ | 7·59 | 8·43 | 9·56 | 8·19 | 10·72 | 6·90 | 10·51 | 7·52 |
| $Al_2O_3$ | 2·35 | 3·02 | 2·28 | 1·72 | 2·46 | 3·02 | 3·19 | 2·45 |
| $FeO^T$ | 78·39 | 78·09 | 75·91 | 80·82 | 78·82 | 81·35 | 78·43 | 83·33 |
| MnO | 0·62 | 0·74 | 0·60 | 0·60 | 0·51 | 0·56 | 0·66 | 0·82 |
| MgO | 1·39 | 1·57 | 1·51 | 1·31 | 1·14 | 1·42 | 0·90 | 1·20 |
| CaO | 0·09 | 0·39 | 0·06 | 0·03 | 0·07 | 0·07 | 0·07 | 0·09 |
| Total | 90·53 | 92·50 | 90·03 | 92·73 | 93·91 | 93·69 | 94·01 | 95·64 |
| $Si^{4+}$ | 0·004 | 0·010 | 0·004 | 0·002 | 0·007 | 0·014 | 0·009 | 0·009 |
| $Ti^{4+}$ | 0·223 | 0·241 | 0·283 | 0·236 | 0·305 | 0·195 | 0·298 | 0·209 |
| $Al^{3+}$ | 0·108 | 0·135 | 0·106 | 0·078 | 0·110 | 0·134 | 0·142 | 0·107 |
| $Fe^{3+}$ | 1·438 | 1·362 | 1·320 | 1·446 | 1·266 | 1·448 | 1·242 | 1·457 |
| $Fe^{2+}$ | 1·122 | 1·122 | 1·176 | 1·143 | 1·229 | 1·109 | 1·233 | 1·122 |
| $Mn^{2+}$ | 0·021 | 0·024 | 0·020 | 0·019 | 0·016 | 0·018 | 0·021 | 0·026 |
| $Mg^{2+}$ | 0·081 | 0·089 | 0·089 | 0·075 | 0·064 | 0·080 | 0·051 | 0·066 |
| $Ca^{2+}$ | 0·004 | 0·016 | 0·003 | 0·001 | 0·003 | 0·003 | 0·003 | 0·004 |
| Total | 3 | 3 | 3 | 3 | 3 | 3 | 3 | 3 |
| Oxygen | 4 | 4 | 4 | 4 | 4 | 4 | 4 | 4 |
| $T$(°C) | 858 | 858 | 858 | 858 | 1049 | 1049 | 1049 | 1049 |
| $\log fO_2$ | −11·2 | −11·4 | −11·7 | −11·3 | −8·1 | −7·3 | −8·1 | −7·5 |
| δFMQ | 2·1 | 1·9 | 1·5 | 2·0 | 2·0 | 2·8 | 2·1 | 2·6 |

Absolute and relative (to the FMQ buffer) oxygen fugacities calculated by the QUILF method, with temperatures from coexisting pyroxenes. Relative oxygen fugacities show only minor dependence on absolute temperature.

Fe. Compositions are magnesio-hastingsites in the Leake *et al.* (1997) classification. Na, K and Ti contents are also much higher than in amphibole in the andesite (Table 4). In some samples, crystals have been partially replaced by a lower-Al amphibole ($Al_2O_3$ between 6·5 and 9%), overlapping in composition with the large andesitic phenocrysts. The framework amphibole in the mafic inclusions generally has very narrow (<20 μm) or no reaction rims. Mafic inclusions in strongly oxidized andesite samples typically contain oxidized framework amphibole.

Pyroxene compositions are similar to those in the groundmass of the andesite (Table 3, Fig. 5). Crystals are heterogeneous with patchy, sector or lamellar zoning, with segments of orthopyroxene and pigeonite or augite and pigeonite.

Titanomagnetite compositions overlap with those in the andesite but extend to higher $TiO_2$ (Table 5). Crystals in oxidized samples are heterogeneous with lamellar exsolution textures. The more pristine mafic inclusions have more homogeneous crystals but there is significant inter-grain variation in individual samples.

## PETROLOGY OF OLDER MONTSERRAT ROCKS

Several older samples from the Soufriere Hills centre have been studied for comparison with the new magma. All of the eruptive products of the Soufriere Hills volcano range between about 58 and 64 wt % $SiO_2$. Mafic inclusions, similar to those in the current andesite, occur in all of the older lavas and pyroclastic deposits. Analyses of lava and a mafic inclusion from the Castle Peak dome (~350 years old) and of samples from pyroclastic deposits (18 ka and 3·7 ka) are given in Table 1. The Castle Peak andesite is similar in bulk composition and mineralogy to the current andesite.

The 3·75 ka and 18 ka samples analysed here are slightly more silicic (62–63·8% $SiO_2$) than the current andesite, but the mineral assemblages are very similar. Plagioclase has a wide range of compositions but large phenocrysts typically have cores between $An_{49}$ and $An_{60}$, as in the current andesite. Type 2 and 3 plagioclase crystals are common but are less abundant than in the current andesite. Amphibole is similar in composition to

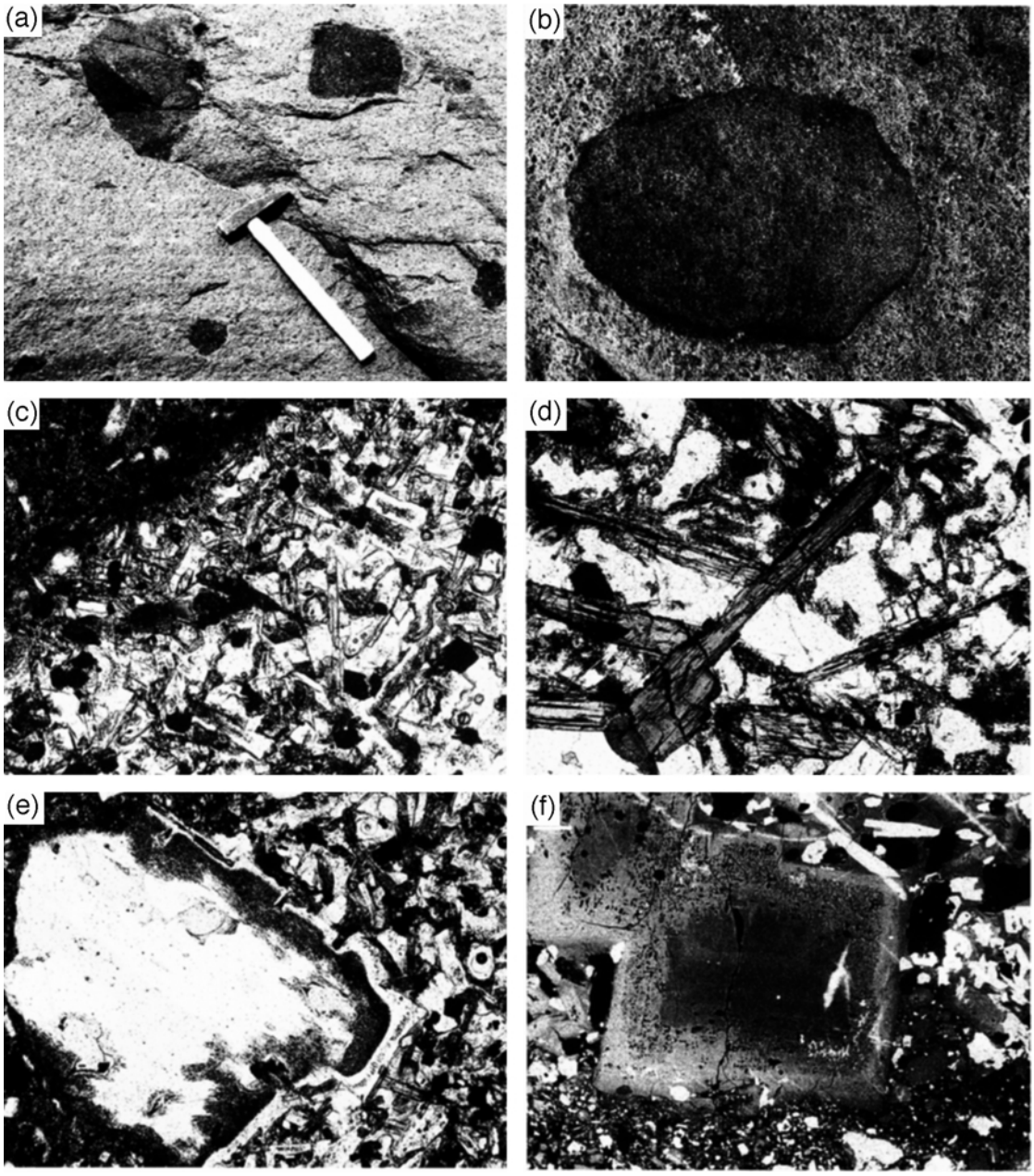


**Fig. 8.** Images of mafic inclusions. Field of view of photomicrographs is 2·5 mm. (a) Mafic inclusions in andesite lava block. Hammer (37 cm) for scale. (b) Large mafic inclusion (15 cm long) in block of older Soufriere Hills andesite with well-developed chilled margin, emphasized by weathering. The inclusion has a crenulated contact with the host andesite. (c) Photomicrograph of fine-grained diktytaxitic groundmass of small (2 cm) mafic inclusion with andesite at top left. The sharp wavy contact should be noted. (d) Photomicrograph of coarse-grained diktytaxitic groundmass of large (20 cm) mafic inclusion. [Compare the grain size with that in (c).] (e) Photomicrograph of sieve-textured plagioclase crystal, which has been partially incorporated into a small (2 cm) fine-grained mafic inclusion. (f) Electronmicrograph of sieve-textured plagioclase crystals partially incorporated into a mafic inclusion (top); 100 μm scale bar at top left.

that in the current andesite. Many orthopyroxenes are similar to those in the current andesite but crystals with much lower Wo contents (averaging 1·3 and ranging between 1·2 and 1·6) are more abundant than in the current andesite.

Mafic samples from the South Soufriere Hills centre (∼125 ka) have an assemblage of plagioclase, olivine, clinopyroxene and titanomagnetite. Plagioclase cores range between $An_{82}$ and $An_{94}$. Olivine invariably has pigeonite rims. Large olivine phenocryst cores range

between $Fo_{81}$ and $Fo_{84}$ and microphenocryst cores range between $Fo_{62}$ and $Fo_{71}$. Clinopyroxene has *mg*-number between 72 and 76. Titanomagnetite is variable in composition but some crystals have relatively high $TiO_2$ contents ($\sim$14%).

## GEOTHERMOMETRY AND OXYGEN BAROMETRY

Andesite magma temperatures have been estimated using the QUILF program of Andersen *et al.* (1993). Because clinopyroxene occurs only as microphenocrysts and microlites and is not in equilibrium with the orthopyroxene phenocrysts, the QUILF program has been used in single pyroxene mode, requiring input of the orthopyroxene composition only. Only phenocryst temperatures are quoted here, as groundmass pyroxenes in the andesite are heterogeneous and give inconsistent results. In single pyroxene mode, the QUILF program calculates a temperature and an equilibrium clinopyroxene composition. The accuracy of this method has been tested using experimentally produced orthopyroxenes. The temperatures of the clinopyroxene-absent experiments of Barclay *et al.* (1998) on Soufriere Hills andesite and of Gardner *et al.* (1995) on Mount St Helens dacite, which has a similar assemblage to the Montserrat andesite, are reproduced to within $\pm$20°C or better in most cases. The thermometer is most sensitive to variations in CaO content of orthopyroxene. Analytical precision for CaO at low abundance levels is about $\pm$0·05%, which translates to an uncertainty in temperature of $\pm$20°C. All values quoted are calculated for a pressure of 1·5 kbar but the variation of the thermometer with pressure is insignificant here (+3–4°C/kbar). The pressure estimate is derived from the requirement that the minimum depth of the magma chamber is about 5–6 km, as amphibole is unstable at shallower depths because of the pressure dependence of water solubility in the magma (e.g. Merzbacher & Eggler, 1984).

The Wo contents of orthopyroxene cores in the current andesite are mostly between 0·019 and 0·023 (0·9–1·1% CaO), corresponding to a range in calculated temperatures of about 40°C. The mean core temperature is 858 $\pm$ 18°C, calculated from 181 analyses of 33 crystals. The overall range is 812–891°C, with most values between 835 and 875°C (Fig. 9a). The rare low-Ca orthopyroxene phenocrysts give values around 750°C. The reverse zoned orthopyroxene rims invariably yield higher values than the cores, ranging between 870 and 1040°C (Fig. 9b). Although the intra-grain compositional variation of the reverse zoned rims is large, individual crystals have more homogeneous rims. The range within individual rims is usually less than 40°C. Orthopyroxene phenocrysts in the older Soufriere Hills andesites (18 500 and 3750 BP) give an average temperature of 861 $\pm$ 16°C. The low-Ca orthopyroxene phenocrysts, which are more abundant in the older samples, give an average temperature of 747 $\pm$ 7°C.

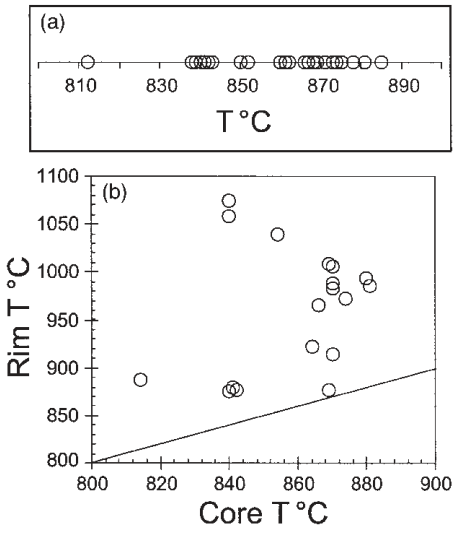


**Fig. 9.** (a) Plot of calculated temperatures of orthopyroxene cores. Each point represents the average composition of a single crystal. The data represent 181 analyses of 31 different crystals. (b) Average rim plotted against average core temperatures of individual reverse zoned orthopyroxene phenocrysts. Each point represents 5–10 analyses of the rims and a similar number of core analyses. All points fall above the 1:1 line.

Oxygen fugacities have also been estimated using the QUILF program. Only the titanomagnetite composition is required for the calculation, as the temperature is constrained by the orthopyroxene composition. The method is advantageous for calculation of oxygen fugacity in magmas such as the Soufriere Hills andesite where ilmenite is present in very minor abundance and it also counteracts problems caused by rapid re-equilibration of Fe–Ti oxides, particularly ilmenite (see Frost & Lindsley, 1992). Compositions of the most homogeneous titanomagnetite crystals were used in the calculations. Estimated relative oxygen fugacities are between 1·5 and 2 log units above QFM (quartz–fayalite–magnetite) with only minor dependence on absolute temperature (Table 5).

The mafic inclusions are believed to represent phenocryst-poor, hydrous basaltic to basaltic andesite magma(s) that intruded the andesite magma reservoir (see below). The temperatures of the inclusion-forming magma(s) are not well constrained. First, the pyroxenes, which occur only in the groundmass, are believed to have crystallized by quenching (see below) and may record quench or re-equilibration rather than original magmatic temperatures. Second, most pyroxenes are heterogeneous, like those in the andesite groundmass, and give unreliable temperature estimates. The most

consistent values are in the range 1020–1060°C, obtained from homogeneous orthopyroxene crystals. However, constraints on the minimum temperatures of the mafic magmas are available from experiments, as the $H_2O$-saturated liquidus temperature of the andesite is about 1050°C at 1·5 kbar (Barclay *et al.*, 1998). The $H_2O$-saturated liquidus temperature of the mafic magmas would be higher than that of the andesite. If the crystal-poor mafic magmas were not $H_2O$ saturated, then they would have had even higher temperatures. Minimum temperatures of 1050°C are consistent with low-pressure liquidus temperatures of hydrous mafic magmas from the literature (e.g. Sisson & Grove, 1993). Relative oxygen fugacities of the mafic inclusion magmas are similar to the andesite values (Table 5) but probably less accurate, because of greater variability in titanomagnetite compositions.

## DISCUSSION

### Magma mingling

The term 'magma mingling' as used here refers to the formation of discrete inclusions by quenching of hotter magma in a lower-temperature magma (see Bacon, 1986). The process of complete mixing of two magmas to form a new magma, commonly containing crystals from the two end-members, is termed 'hybridization'.

The evidence for magma mingling in the current Soufriere Hills andesite is unequivocal. The mafic inclusions are interpreted as quenched blobs of hydrous mafic magma at temperatures of around 1050°C or above, which have been intruded into cooler andesite magma at about 850°C. In itself, the occurrence of xenocrysts derived from the andesite, in some cases partially incorporated into the inclusions, demonstrates that the mafic inclusions must have been molten when formed. The quench-textured groundmasses, ellipsoidal shapes, crenulate contacts and chilled margins are all characteristic of magmatic mafic inclusions (Vernon, 1983; Bacon, 1986; Sparks & Marshall, 1986; Blundy & Sparks, 1992). The acicular character of crystals is indicative of rapid cooling rates (Lofgren, 1980). The increase in crystal size and change in crystal shape from acicular to more prismatic and equant shapes as the inclusion size increases can also be attributed to slower cooling in larger inclusions. The tendency for pyroxene to be more abundant than amphibole in small inclusions can be explained by a variety of mechanisms including preferential loss of water from small inclusions promoting pyroxene stability or possible kinetic effects related to more rapid cooling of small inclusions.

The whole-rock chemistry of the inclusions suggests that they represent quenched basaltic to basaltic andesite magma(s), with compositions similar to the South Soufriere Hills lavas. The low MgO contents and very low Ni and Cr contents suggest that the mafic magmas have experienced extensive fractionation following their presumed generation in the mantle.

Magma mingling rather than hybridization is dominant, as the inclusions generally remain coherent and have sharp contacts with the host andesite. Rarely, there is evidence for minor disaggregation and subsequent hybridization, where the mafic inclusion groundmass minerals form local streaks into the andesite near the margins of inclusions. However, there is no evidence for significant disaggregation of inclusions in a partially molten state, in contrast to, for example, the situation described by Clynne (1999) for material erupted in 1915 at Lassen Peak, California. If the inclusions had disaggregated and hybridized with the andesite, groundmass minerals that had formed within the inclusions should be present in the andesite groundmass. This is not observed. First, groundmass amphibole is completely absent from the andesite whereas it is abundant in most inclusions. Second, the compositions of groundmass plagioclase in the andesite are distinct from those in the inclusions (Fig. 3). Third, the morphologies of microphenocryst and microlite pyroxenes in the andesite are distinct from those in the mafic inclusions, the latter commonly having elongate to acicular forms and the former being more equant. Although significant disaggregation of partially molten inclusions can therefore be ruled out, it is likely that inclusions with one or more angular faces formed by brecciation of solidified larger inclusions. However, this process did not result in hybridization.

The predominance of mingling over hybridization at Montserrat can be related to the large contrast in temperature and viscosity between the cool, crystal-rich andesite and the hot, crystal-poor mafic magma, and to small proportions of mafic magma in the mixture, which results in rapid quenching of the mafic magma at temperatures close to that of the andesite host (Sparks & Marshall, 1986).

The andesite also shows abundant evidence for reheating and recrystallization at higher temperatures. Reverse zoned dusty sieve-textured plagioclase, similar to that in the Soufriere Hills andesite and mafic inclusions, has been reported from many mingled and hybrid magmas (Eichelberger, 1978; Heiken & Eichelberger, 1980; Gerlach & Grove, 1982; Kawamoto, 1992). The texture can form by reheating plagioclase above its equilibrium solidus temperature but below its liquidus. Rapid recrystallization occurs, producing a very fine-grained intergrowth of more calcic plagioclase and trapped glass. Laboratory experiments have produced similar textures (Tsuchiyama, 1985; Nakamura & Shimakita, 1996).

The reverse zoned rims on many orthopyroxene phenocrysts, which give significantly higher calculated temperatures than the cores, also indicate reheating of the magma. The calcic rims of simply reverse zoned, unresorbed, plagioclase phenocrysts and the calcic microphenocrysts can also be interpreted in terms of rising magma temperature. The rounding of quartz crystals and the presence of fine-grained clinopyroxene rims may also be related to reheating of the magma.

Some of the amphibole reaction textures may also have been produced by reheating of the magma. Rounding of some amphibole crystals may be caused by resorption as a result of reheating. Although the fine-grained rims (Type 1) on many amphibole phenocrysts in the andesite are likely to be formed by volatile loss from the magma during ascent (Devine *et al.*, 1998*a*), some of the fine-grained replacement textures may also have formed as a consequence of reheating. Xenocrysts in mafic inclusions have very fine-grained reaction products that have extensively replaced the original crystal and these textures are difficult to distinguish from decompression-induced reaction textures. The coarse-grained reaction textures (Type 2) may also have formed by reheating.

## History of the Soufriere Hills magma chamber

The detailed eruptive history of the Soufriere Hills centre is currently not well constrained and the following discussion is based on a small set of samples of known eruption ages from 18 ka to the present.

Several features suggest that the current andesite may be derived from a relatively old, highly crystalline magma body. First, all magmas erupted over the last 18 kyr at least are crystal rich, have very similar mineral chemistry and a restricted range in bulk compositions ($\sim$58–64 wt % $SiO_2$). Second, simple least-squares mass balance calculations, using typical crystal compositions (Tables 2–5) and glass compositions from Devine *et al.* (1998*b*) indicate that the magma was highly crystalline (at least 60–65 wt %) in the magma chamber before eruption, further crystallization of microlites occurring during ascent. Third, the calculated magma temperature of 860°C is about 200°C below the experimentally determined water-saturated liquidus temperature of 1050°C at 1·5 kbar (Barclay *et al.*, 1998). The high crystallinity and low temperature indicate that the magma has experienced a protracted cooling history, which, together with the similarity in mineral chemistry and narrow range in bulk chemistry of all magmas erupted over the last 18 kyr, indicates that all eruptions may be tapping the same magma body. This interpretation is supported by preliminary U–Th results on mineral separates from the current and 3·75 ka rocks, which give dates of 25 $\pm$ 10 ka (Murphy *et al.*, 1998).

In this interpretation, the magma has existed as a highly crystalline body with pluton-like mechanical properties, remaining at a temperature of about 860 $\pm$ 20°C for the last 18 kyr at least, with periodic perturbations in temperature as a result of influx of hotter mafic magma, inferred from the presence of mafic inclusions, similar to those in the current andesite, in all of the older products of the Soufriere Hills volcano. Periodic replenishment by fresh mafic magma prevents the resident magma from fully crystallizing and may result in eruption, as discussed below. Each intrusive episode involves non-uniform reheating of the magma body, which may subsequently return to steady low-temperature ($\sim$860°C) state and continue to crystallize a low-temperature mineral assemblage.

## Causes of magma heterogeneity

A prominent feature of the Soufriere Hills andesite is microscale heterogeneity, which is manifested by juxtaposition of crystals that record different petrogenetic histories. Diversity in compositions, zoning patterns and textures of the phenocryst phases indicates that these crystals have been mixed together from widely different magmatic environments. The key question is what these variations in crystal history imply about spatial and temporal variations in magma composition, volatile content and temperature. We interpret the observations in the context that the mafic magma, as represented by the mafic inclusions, can provide heat, mass and volatiles to the andesite magma.

The variations in rim compositions, zoning patterns and extent of resorption of plagioclase phenocrysts and the range in plagioclase microphenocryst compositions indicate that individual crystals have experienced different thermal histories. Similarly, the narrow variations in rim compositions of individual reverse zoned orthopyroxene crystals, together with the wide inter-grain range in the compositions of the reverse zoned rims, indicate that different crystals have experienced different degrees of reheating. The amount of reheating experienced by an individual crystal will depend on its proximity to the intruding mafic magma. Temperatures over 1000°C may have been reached locally, as the mafic magma is estimated to have been at a temperature of at least 1050°C. However, the overall temperature of the andesitic magma body cannot have reached more than about 880°C, as amphibole remains as a stable phase. The experiments of Barclay *et al.* (1998) show that amphibole becomes unstable at about 880°C. The evidence thus points to parts of the andesite having been reheated by intrusion of mafic magma to temperatures well above the original temperature at which the stable phenocryst assemblage of sodic plagioclase ($\sim An_{48-58}$), orthopyroxene, amphibole and titanomagnetite formed.

Localized, non-uniform reheating of the andesite magma by intrusion of hotter mafic magma is likely to be a consequence of the highly crystalline nature of the resident magma. The minimum crystallinity of the magma in the reservoir can be estimated from mass balance calculations to be about 60–65 wt %, which is close to the volume percent critical crystallinity at which magmas behave as solids rather than liquids (Marsh, 1981; Lejeune & Richet, 1995). Therefore, before reheating, the andesitic magma body would have been so highly crystalline that its physical properties are more aptly considered in terms of a rigid, immobile, partially molten pluton than of a mobile magma (see Marsh, 1981; Furman & Spera, 1985). Mafic magma can intrude into the still rigid highly crystalline andesite magma body, forming dykes or sills that are subsequently broken up to form quenched mafic inclusions as the host is heated and softens (Blake, 1966; Blundy & Sparks; 1992; Hallot *et al.*, 1996).

Several processes may have contributed to inclusion formation. Angular inclusions are likely to represent fragments of larger inclusions, dykes or sills that have disintegrated in a solid or near-solid state. Rounded inclusions are likely to represent quenched blebs of magma that have been incorporated into the host in a liquid or near-liquid state, as evidenced by the relationship between inclusion size and groundmass grain size and by the presence of chilled margins on some inclusions. Mechanisms that have been invoked to explain the latter process elsewhere include forcible injection of mafic magma (Turner & Campbell, 1986) and buoyant uprise of vesiculated underplated mafic magma into an overlying more silicic host (Eichelberger, 1980).

A major paradox of remobilization of crustal magma bodies is that crystallization takes place simultaneously with melting, when the system is considered on a large scale. Huppert & Sparks (1988) presented basic fluid dynamical principles that govern the interactions when crustal rocks or, as envisaged here, a highly crystalline magma body are remobilized. Although Huppert & Sparks (1988) considered the case of a sill, the main principles are generic and do not depend on the detailed geometrical relationships. Initially, when the mafic magma intrudes, heating is localized so that a large amount of heat is transferred into a relatively small body of host rock or magma. Once the temperature exceeds a threshold value where the melt content is sufficiently high that the mechanical strength is lost, convection begins. Thus a mobile magma body forms, surrounded by partially molten, immobile magma. Melting reactions take place at the rheologically determined boundary between mobile magma and partially molten material, which still behaves mechanically as a solid. The threshold condition is usually considered to be around 60–70 vol. % crystals (Marsh, 1981; Huppert & Sparks, 1988; Lejeune & Richet, 1995). As the volume of mobile magma grows, its average temperature falls with time and it begins to crystallize. Thus, counter-intuitively, simultaneous melting and crystallization are a consequence of the fluid dynamical principles.

There are no definite constraints on the precise mechanism(s) of inclusion formation at Montserrat but the following model, illustrated schematically in Fig. 10, can explain the observations. Initial intrusion of mafic magma results in underplating of a hot mafic magma beneath the less dense resident magma and formation of mafic dykes in the highly crystalline andesite. Softening of the host andesite by reheating and partial melting permits formation of elliptical inclusions by buoyant uprise or forcible injection of hot liquid as more mafic magma intrudes. Forced convection within the andesite results in fragmentation of earlier-formed dykes to form angular inclusions.

The heterogeneous character of the Soufriere Hills andesite mineral assemblage can be simply explained by such a model. Initially, material that is close to the locus of mafic intrusions can be heated to high temperature, approaching that of the mafic magma itself. High-temperature orthopyroxene rims and resorbed sieve-textured plagioclase may represent regions of the remobilized magma that reached very high temperatures. As the remobilized magma body grows and cools, similar crystals in the original host are less dramatically affected. Falling temperature also results in formation of overgrowth rims on plagioclase and orthopyroxene and growth of the microphenocryst assemblage. As the magma body approaches temperatures and crystal contents that are comparable with the rheological critical conditions where rigidity sets in, the last crystals to be swept into the magma may grow no fresh rims at all.

The above model will be complicated by two factors. First, the region being remobilized may itself have compositional and thermal gradients. The lower-temperature ($\sim$750°C) orthopyroxene crystals, which occur in samples from all eruptions but are rare in the current andesite, may represent material from a cooler nearly solidified part of the chamber, towards the roof or walls. The quartz crystals may also be derived from a relatively cool and highly crystalline marginal part of the system. Quartz is stable in the Soufriere Hills andesite only at or below about 830°C (Barclay *et al.*, 1998) and contains high-Si rhyolite melt inclusions (76–79% $SiO_2$) that are generally more evolved than the groundmass glass, suggesting that parts of the magma chamber had reached a very advanced state of crystallization. Given that most orthopyroxene temperature estimates are significantly higher than 830°C, the maximum temperature at which quartz is stable in the andesite, it is likely that the reservoir was thermally zoned before influx of the mafic magma.

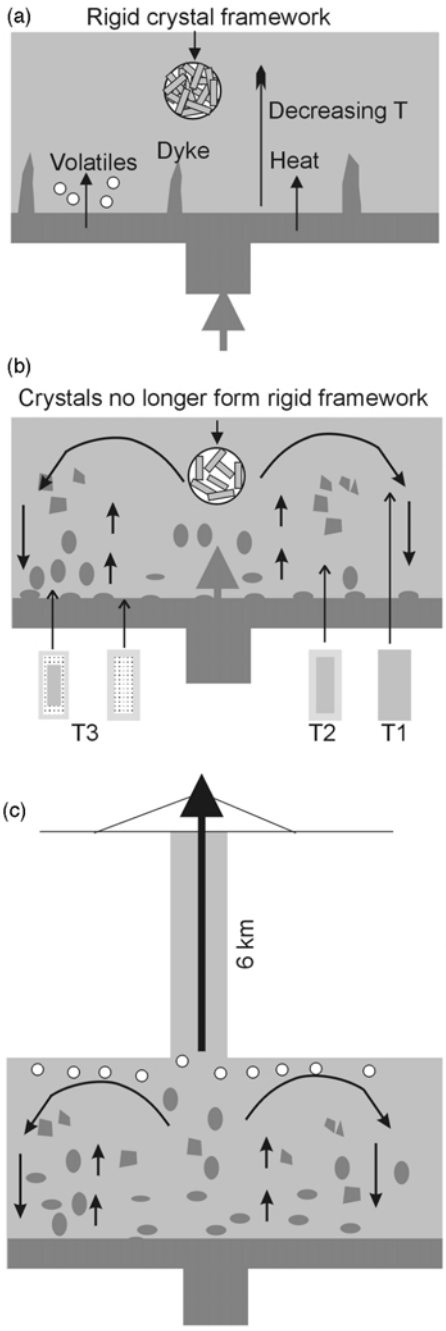


**Fig. 10.** Schematic diagram illustrating the main features of the model discussed in the text. (a) Initial intrusion of mafic magma into highly crystalline, near-plutonic andesitic magma body. Underplating of denser mafic magma and dyke intrusion. Addition of heat and volatiles from mafic magma. Temperature gradient set up in resident magma. (b) Partial melting of resident crystals together with reheating and addition of volatiles lowers viscosity of resident magma. Thermal convection begins, disrupting dykes and mixing crystals from different parts of the resident magma together. Mafic inclusions form as fragments of disrupted dykes and as quenched blobs of mafic liquid by forceful intrusion and/or buoyant uprise of vesiculated mafic magma. (c) Pressurization of magma chamber by build-up of volatiles leads to eruption.

A second cause of variation is the extent to which melt, crystals and volatiles are transferred from the mafic magma. In general, the extent of hybridization appears to be very minor and localized to areas adjacent to mafic inclusions. Highly calcic plagioclase crystals, which are likely to represent xenocrysts derived from the mafic magma, are rare in the andesite. However, volatile transfer from the mafic magma to the host andesite is probable and may be significant. The mafic inclusions represent volatile-rich magma, evidenced by the presence of amphibole and their high vesicularity. The volatile budget in the andesite is controlled by two counteracting effects. Rhyolitic melt inclusions in quartz and plagioclase contain 4–5 wt % $H_2O$ (Barclay *et al.*, 1998; Devine *et al.*, 1998*b*) implying $H_2O$-saturated conditions in the residual melt at 1·25–1·5 kbar. Melting of predominantly anhydrous crystals in the andesite will tend to produce a water-undersaturated melt. On the other hand, transfer of volatiles from the hydrous mafic magma can elevate $H_2O$ contents and even create an excess vapour phase. Thus, $P(H_2O)$ can fluctuate with time and position, affecting local liquidus relations and compositions of overgrowth rims.

We conclude, therefore, that mineral heterogeneity in the andesite is caused by convective mixing together of crystals that have experienced different histories both before and during replenishment of the magma reservoir by hot mafic magma.

## Intrusion of mafic magma as an eruption trigger

The effect of intrusion of hot magma into a cooler magma reservoir is widely recognized as a potential eruption trigger (e.g. Sparks *et al.*, 1977; Pallister *et al.*, 1992; Eichelberger, 1995). There are several possible effects of addition of hot mafic magma to a reservoir containing cooler silicic magma. The simple addition of a new volume of magma to the magma chamber causes pressurization, which may lead to fracturing of the roof and ascent of magma, possibly leading to eruption. Heating of the resident magma causes exsolution of volatiles, which can also cause pressurization of the chamber. Heating can also force convective uprise of the resident magma. Transfer of volatiles from the mafic magma to the silicic magma can also contribute to pressurization of the magma chamber. All of these effects may combine to initiate a new eruption, following an intrusive episode.

There is no direct constraint on the timing of recent mafic magma intrusion events beneath the Soufriere Hills volcano, as the mafic inclusions in the current andesite may not necessarily represent magma that was recently intruded. However, the freshness of many of the inclusions and the lack of evidence from mineral compositions for

re-equilibration in most of the inclusions analysed suggest that the inclusions have formed recently. The presence of compositional banding in some samples also suggests very recent convective stirring. Further evidence for recent intrusion of mafic magma is provided by the mineral chemistry of the andesite. In particular, the increase in width of reverse zoned rims on orthopyroxene phenocrysts over the course of the eruption suggests that these rims have grown very recently, as a result of reheating of the magma. The presence of calcic rims on many plagioclase phenocrysts and the abundance of calcic microphenocrysts also suggest that recent mafic magma intrusion has occurred.

The precursor seismicity, which began in 1992, may have been initiated by movement of magma from levels deep (at least 14 km) within the crust, according to a preliminary interpretation of the geophysical data (Young *et al.*, 1998*b*). This may therefore reflect an intrusive pulse of mafic magma into a shallow magma chamber at about 6–7 km depth. Evidence for the existence of a shallow magma chamber comes from geophysical data recorded throughout the eruption, which locate a large number of earthquakes at about 5–7 km depth (Aspinall *et al.*, 1998). Other seismic crises at about 30 year intervals over the last 100 years may also reflect movement of mafic magma from deep levels in the crust, intruding the shallow magma chamber. Although these events did not lead directly to eruptions, some of the mafic inclusions in the current andesite may have been formed at these times. Addition of mass and heat to the magma chamber during these earlier events may have primed the resident magma for eruption, and the recent intrusion may have acted as the final trigger.

Evidence for the eruption being driven by influx of mafic magma also comes from extrusion rate and $SO_2$ gas flux data. The magma extrusion rate increased with time, from 0·5 $m^3/s$ in the first few weeks of activity, averaging 2·3 $m^3/s$ in 1996 and accelerating to about 6–7 $m^3/s$ between May 1997 and February 1998. Dome growth then stopped abruptly in early March 1998. This is the opposite trend to that expected in a closed-system pressurized magma chamber (Sparks *et al.*, 1998). The behaviour can be explained by an open-system model, in which influx of new mafic magma has maintained or even increased chamber pressure with time. This interpretation requires a volume of new mafic magma comparable with the amount of andesite extruded. The mafic inclusions can represent only a tiny fraction of the new mafic magma. We surmise that a much larger volume of new mafic magma was emplaced beneath the andesite magma body during the eruption.

This model is further supported by gas flux studies. Studies of $SO_2$ fluxes show that there an excess sulphur problem (Young *et al.*, 1998*a*), the $SO_2$ flux being somewhat higher than can be accounted for by degassing of the andesite. For example, melt inclusion studies suggest only about 100–150 ppm S was dissolved in the rhyolitic melt phase. At the observed extrusion rates, this amount of dissolved $SO_2$ is enough to sustain fluxes of only a few tens of tons per day, whereas the observed fluxes are many hundreds to about 2000 tons/day (Young *et al.*, 1998*a*). The source of the excess $SO_2$ can be explained by influx of mafic magma, which releases dissolved volatiles as it cools and crystallizes.

## CONCLUSIONS

The andesite magma currently erupting at the Soufriere Hills volcano, Montserrat, shows unequivocal evidence for open-system behaviour with influx of mafic magma into a crystal-rich andesite host. Mafic inclusions show evidence of being molten during incorporation into the andesite and are believed to represent quenched blobs and fractured dykes of mafic magma that was intruded into the andesite. Crystals in the andesite record a complex history of growth and resorption. Calculated andesite magma temperatures from pyroxene geothermometry are about 200°C below the water-saturated liquidus but reverse zoned rims record a recent reheating event. The crystal-rich nature of the andesite, the low temperatures and the similarity in mineral compositions over the last 18 kyr are interpreted in terms of a long-lived, relatively cool magma chamber. The resident magma is at least 60–65% crystalline and has pluton-like physical properties. Periodic intrusion of mafic magma results in reheating and remobilization of the resident magma. Phenocrysts in the andesite, which is itself thermally zoned before the mafic influx, experience different degrees of resorption and recrystallization under locally variable conditions, depending on their proximity to intruding mafic bodies. Remobilization results in the mixing together of andesitic phenocrysts that record complex and variable histories. The current eruption is believed to have been triggered by a recent intrusion of mafic magma from deep crustal levels, reflected in the seismic crisis that began more than 3 years before the eruption.

## ACKNOWLEDGEMENTS

This paper is published by permission of the Director, British Geological Survey (NERC). Dr Simon Young of the British Geological Survey and members of the Montserrat Volcano Observatory are acknowledged for providing many of the samples used in this study, many of which were collected under dangerous conditions. Dr Joe Devine of Brown University, Providence, RI, USA, is acknowledged for detailed discussion of the petrology of the Soufriere Hills rocks. The thorough and constructive

reviews of an earlier draft of this manuscript by Dr Mike Clynne, Dr John Gamble and Dr John Eichelberger are gratefully acknowledged. The research was supported by NERC Grants GR3/10679 and GR3/11020. Funding from the UK Department for International Development is also acknowledged.

## REFERENCES

Andersen, D. J., Lindsley, D. H. & Davidson, P. M. (1993). QUILF: a PASCAL program to assess equilibria among Fe–Mg–Ti oxides, pyroxenes, olivine and quartz. *Computers and Geosciences* **19**, 1333–1350.

Aspinall, W. P., Miller, A. D., Lynch, L. L., Latchman, J. L., Stewart, R. C., White, R. A. & Power, J. A. (1998). Soufriere Hills eruption, Montserrat, 1995–1997: volcanic earthquake locations and fault plane solutions. *Geophysical Research Letters* **25**, 3397–3400.

Bacon, C. R. (1986). Magmatic inclusions in silicic and intermediate volcanic rocks. *Journal of Geophysical Research* **91B**, 6091–6112.

Baker, P. (1984). Geochemical evolution of St. Kitts and Montserrat, Lesser Antilles. *Journal of the Geological Society, London* **141**, 401–411.

Barclay, J., Carroll, M. R., Rutherford, M. J., Murphy, M. D., Devine, J. D., Gardner, J. & Sparks, R. S. J. (1998). Experimental phase equilibria constraints on pre-eruptive storage conditions of the Soufriere Hills magma. *Geophysical Research Letters* **25**, 3437–3440.

Baxter, P. J., Bonadonna, C., Dupree, R., Hards, V. L., Kohn, S. C., Murphy, M. D. *et al.* (1999). Cristobalite in volcanic ash of the Soufriere Hills volcano, Montserrat: hazards implications. *Science* **283**, 1142–1145.

Blake, S. (1966). The net-veined complex of the Austurhorn intrusion, southeastern Iceland. *Journal of Geology* **74**, 891–907.

Blundy, J. D. & Sparks, R. S. J. (1992). Petrogenesis of mafic inclusions in granitoids of the Adamello Massif. *Journal of Petrology* **33**, 1039–1104.

Clynne, M. A. (1999). A complex magma mixing origin for rocks erupted in 1915, Lassen Peak, California. *Journal of Petrology* **40**, 105–132.

Devine, J. D., Gardner, J. & Rutherford, M. J. (1998*a*). Petrologic determination of magma ascent rates for the 1995–1997 Soufriere Hills volcano andesitic magma. *Geophysical Research Letters* **25**, 3673–3676.

Devine, J., Murphy, M. D., Rutherford, M., Barclay, J., Sparks, R. S. J., Carroll, M. R. *et al.* (1998*b*). Petrological evidence for pre-eruptive pressure–temperature conditions of andesitic magma erupting at the Soufriere Hills volcano, Montserrat, W.I. *Geophysical Research Letters* **25**, 3669–3672.

Eichelberger, J. C. (1978). Andesitic volcanism and crustal evolution. *Nature* **275**, 21–27.

Eichelberger, J. C. (1980). Vesiculation of mafic magmas during replenishment of silicic magma reservoirs. *Nature* **288**, 446–450.

Eichelberger, J. C. (1995). Silicic volcanism: ascent of viscous magmas from crustal reservoirs. *Annual Review of Earth and Planetary Science* **23**, 41–63.

Frost, B. R. & Lindsley, D. H. (1992). Equilibria among Fe–Ti oxides, pyroxenes, olivine, and quartz: Part II. Application. *American Mineralogist* **77**, 1004–1020.

Furman, T. & Spera, F. J. (1985). Co-mingling of acid and basic magma with implications for the origin of mafic I-type xenoliths: field and petrochemical relations of an unusual dike complex at Eagle Lake, Sequoia National Park, California, U.S.A. *Journal of Volcanology and Geothermal Research* **24**, 151–178.

Garcia, M. O. & Jacobson, S. (1979). Crystal clots, amphibole fractionation and the evolution of calc-alkaline magmas. *Contributions to Mineralogy and Petrology* **69**, 319–327.

Gardner, J. E., Rutherford, M., Carey, S. & Sigurdsson, H. (1995). Experimental constraints on pre-eruptive water contents and changing magma storage prior to explosive eruptions of Mount St Helens volcano. *Bulletin of Volcanology* **57**, 1–17.

Gerlach, D. C. & Grove, T. L. (1982). Petrology of Medicine Lake Highland Volcanics: characterisation of end-members of magma mixing. *Contributions to Mineralogy and Petrology* **80**, 147–159.

Gill, J. B. (1981). *Orogenic Andesites and Plate Tectonics*. Berlin: Springer.

Hallot, E., Davy, P., Dars, J. D., Auvray, B., Martin, H. & Vandamme, H. (1996). Non-newtonian effects during injection in partially crystallized magmas. *Journal of Volcanology and Geothermal Research* **71**, 31–44.

Harvey, P. K., Lovell, M. A., Brewer, T. S., Locke, J. & Mansley, E. (1996). Measurement of thermal neutron absorption cross section in selected geochemical reference materials. *Geostandards Newsletter* **20**, 79–85.

Holland, T. J. B. & Blundy, J. D. (1994). Non-ideal interactions in calcic amphiboles and their bearing on amphibole–plagioclase thermometry. *Contributions to Mineralogy and Petrology* **116**, 433–447.

Heiken, G. & Eichelberger, J. C. (1980). Eruptions at Chaos Crags, Lassen Volcanic National Park, California. *Journal of Volcanology and Geothermal Research* **7**, 443–481.

Huppert, H. E. & Sparks, R. S. J. (1988). The generation of granitic magmas by intrusion of basalt into continental crust. *Journal of Petrology* **29**, 599–624.

Kawamoto, T. (1992). Dusty and honeycomb plagioclase: indicators of processes in the Uchino stratified magma chamber, Isu Peninsula, Japan. *Journal of Volcanology and Geothermal Research* **49**, 191–208.

Leake, B. E., Woolley, A. R., Arps, C. E. S., Birch, W. D., Gilbert, M. C., Grice, J. D. *et al.* (1997). Nomenclature of amphiboles: report of the subcommittee on amphiboles of the International Mineralogical Association, commission on new minerals and mineral names. *American Mineralogist* **82**, 1019–1037.

Lejeune, A.-M. & Richet, P. (1995). Rheology of crystal-bearing silicate melts: an experimental study at high viscosities. *Journal of Geophysical Research* **100**, 4215–4229.

Lofgren, G. (1980). Experimental studies on the dynamic crystallisation of silicate melts. In: Hargreaves, R. B. (ed.) *Physics of Magmatic Processes*. Princeton, NJ: Princeton University Press, pp. 487–551.

Marsh, B. D. (1981). On the crystallinity, probability of occurrence and rheology of lava and magma. *Contributions to Mineralogy and Petrology* **78**, 85–98.

Merzbacher, C. & Eggler, D. H. (1984). A magmatic geohygrometer–application to Mount St. Helens and other dacitic magmas. *Geology* **12**, 587–590.

Miyashiro, A. (1974). Volcanic rock series in island arcs and active continental margins. *American Journal of Science* **274**, 321–355.

Murphy, M. D., Sparks, R. S. J., Barclay, J., Carroll, M. R., Lejeune, A.-M., Brewer, T. S. *et al.* (1998). The role of magma mixing in triggering the current eruption at the Soufriere Hills volcano, Montserrat, WI. *Geophysical Research Letters* **25**, 3433–3436.

Nakamura, M. & Shimakita, S. (1996). Partial dissolution kinetics of plagioclase: implication for magma mixing time scale and origin of melt inclusions. *EOS Transactions, American Geophysical Union* **77**(46), F841.

Pallister, J. S., Hoblitt, R. P. & Reyes, A. G. (1992). A basalt trigger for the 1991 eruptions of Pinatubo Volcano. *Nature* **356**, 426–428.

Powell, C. F. (1938). The Royal Society expedition to Montserrat, B.W.I.: Final Report. *Philosophical Transactions of the Royal Society of London, Series A* **158**, 232–252.

Rea, W. J. (1974). The volcanic geology and petrology of Montserrat, British West Indies. *Journal of the Geological Society, London* **130**, 341–366.

Robertson, R., Cole, P. D., Sparks, R. S. J., Lejeune, A.-M., Maguire, W. J., Miller, A. *et al.* (1998). The explosive eruption of Soufriere Hills Volcano, Montserrat, September 17, 1996. *Geophysical Research Letters* **25**, 3429–3432.

Rutherford, M. J. & Hill, P. M. (1993). Magma ascent rates from amphibole breakdown—an experimental study applied to the 1980–1986 Mount St. Helens eruptions. *Journal of Geophysical Research* **98**, 19667–19685.

Shepherd, J. B., Tomblin, J. F. & Wood, D. F. (1971). Volcanoseismic crisis in Montserrat, West Indies, 1966–67. *Bulletin of Volcanology* **35**, 143–163.

Sisson, T. W. & Grove, T. L. (1993). Experimental investigations of the role of $H_2O$ in calc-alkaline differentiation and subduction zone magmatism. *Contributions to Mineralogy and Petrology* **113**, 143–166.

Sparks, R. S. J. & Marshall, L. A. (1986). Thermal and mechanical constraints on mixing between mafic and silicic magmas. *Journal of Volcanology and Geothermal Research* **29**, 99–124.

Sparks, R. S. J., Sigurdsson, H. & Wilson, L. (1977). Magma mixing: a mechanism for triggering acid explosive eruptions. *Nature* **267**, 315–318.

Sparks, R. S. J., Young, S. R., Barclay, J., Calder, E. S., Cole, P. D., Darroux, B. *et al.* (1998). Magma production and growth of the lava dome of the Soufriere Hills Volcano, Montserrat, West Indies: November 1995 to December 1997. *Geophysical Research Letters* **25**, 3421–3424.

Tsuchiyama, A. (1985). Dissolution kinetics of plagioclase in the melt of the system diopside–albite–anorthite, and origin of dusty plagioclase in andesite. *Contributions to Mineralogy and Petrology* **89**, 1–16.

Turner, J. S. & Campbell, I. H. (1986). Convection and mixing in magma chambers. *Earth-Science Reviews* **23**, 255–352.

Vernon, R. H. (1983). Microgranitoid enclaves in granites—globules of hybrid magma quenched in a plutonic environment. *Nature* **309**, 438–439.

Young, S. R., Francis, P. W., Barclay, J., Casadevall, T. J., Gardner, C. A., Darroux, B. *et al.* (1998*a*). Monitoring $SO_2$ emission at the Soufriere Hills volcano: implications for changes in eruptive conditions. *Geophysical Research Letters* **25**, 3681–3684.

Young, S. R., Sparks, R. S. J., Aspinall, W. P., Lynch, L. L., Miller, A. D., Robertson, R. E. A. & Shepherd, J. (1998*b*). Overview of the eruption of the Soufriere Hills volcano, Montserrat, July 18, 1995 to December 1997. *Geophysical Research Letters* **25**, 3389–3392.